THE INFLUENCES OF SEA-SURFACE TEMPERATURE UNCERTAINTY ON COOL-SEASON HIGH-SHEAR, LOW CAPE SEVERE WEATHER EVENT PREDICTABILITY IN THE SOUTHEAST UNITED STATES

by

Michelle Rose Spencer

A Thesis Submitted in

Partial Fulfillment of the

Requirements for the Degree of

Master of Science

in Atmospheric Sciences

at

The University of Wisconsin-Milwaukee

December 2021

ABSTRACT

THE INFLUENCES OF SEA-SURFACE TEMPERATURE UNCERTAINTY ON COOL-SEASON HIGH-SHEAR, LOW CAPE SEVERE WEATHER EVEN PREDICTABILITY IN THE SOUTHEAST UNITED STATES

by

Michelle Rose Spencer

The University of Wisconsin-Milwaukee, 2021
Under the Provisions of Professor Clark Evans

Environments conducive to severe weather and tornadoes occur throughout the southeastern United States, particularly during the cold-season. Throughout the cold-season, severe weather in this region predominantly occurs in environments characterized by high-shear, low-CAPE (HSLC). An important aspect to the production of severe weather in HSLC environments in the southeast United States is that air parcels that help contribute to the limited positive-buoyancy generation originate over areas such as the Gulf of Mexico, western Caribbean Sea, and western Atlantic Ocean. These relatively warm bodies of water, particularly outside of the cooler coastal shelf regions, allow the air parcels to warm and moisten via latent heat and surface sensible fluxes. It is hypothesized that the forecasts of cold-season severe weather in the southeastern United States are sensitive to the treatment of the underlying ocean surface, which influences the simulated representation of the surface heat exchange between the air and sea. We aimed to address and quantify these sensitivities by conducting numerical simulations for eight identified cold-season southeastern United States severe weather cases initialized using several different sea-surface temperature (SST) analyses. An ensemble of forecasts using varying atmospheric and SST analyses is also conducted for the case with the largest variability in forecast skill between

SST initializations to quantify the contributions of initial atmospheric and SST uncertainty to subsequent forecast uncertainty. Neighborhood-based forecast verification techniques based off updraft helicity swaths are used to quantify these uncertainties.

TABLE OF CONTENTS

LIST OF FIGURES

LIST OF TABLES

LIST OF ABBREVIATIONS

AGL	Above Ground Level
CAM	Convection Allowing Model
CAPE	Convective Available Potential Energy
DTE	Difference Total Energy
FNMOC	Fleet Numerical Meteorology and Oceanography Center
FSS	Fraction Skill Score
GHRSST	Group for High-Resolution Sea-Surface Temperature
HRRR	High-Resolution Rapid Refresh
HSLC	High-Shear, Low-CAPE
LLJ	Low-Level Jet
LSR	Local Storm Report
MUCAPE	Most Unstable Convective Available Potential Energy
NAM	North American Mesoscale
NOAA/OI	National Oceanic and Atmospheric Association
NWS	National Weather Service
QLCS	Quasi-Linear Convective System
REMSS	Remote Sensing Systems
RM-DTE	Root-Mean Difference Total Energy
SBCAPE	Surface-Based Convective Available Potential Energy
SPC	Storm Prediction Center
SST	Sea-Surface Temperature
UH	Updraft Helicity

USNO	US Naval Oceanographic
WFO	Weather Forecast Office
WRF-ARW	Advanced Research Weather Research and Forecasting

1. Introduction

Environments conducive to severe weather and tornadoes occur throughout the United States on a year-round basis. While strong vertical wind shear is typically needed for severe thunderstorms that can produce strong winds, large hail, and tornadoes, there can be a drastic amount of variance in the amount of convective available potential energy (CAPE) in severe environments (e.g., Schneider et al. 2006; Schneider and Dean 2008; Grams et al. 2012; Thompson et al. 2012; Anderson-Frey et al. 2016). Most previous studies of severe weather environments have focused on high-shear, high-CAPE environments, such as those commonly seen over the Great Plains in the late spring and early summer months. However, several recent studies have examined high-shear, low-CAPE (HSLC) environments, commonly found in the eastern United States and during the cool season (Sherburn and Parker 2014; Sherburn et al. 2016; Anderson-Frey et al. 2019). HSLC environments are characterized by large vertical wind shear magnitudes (0-6 km vertical wind shear magnitude $\geq$ 18 m s^{-1}) and low surface-based and most-unstable parcel buoyancy (SBCAPE $\leq$ 500 J kg^{-1} and MUCAPE $\leq$ 1000 J kg^{-1}).

These HSLC environments pose a severe-weather forecasting challenge to operational forecasters, especially in the southeastern United States. While HSLC environments are a frequent occurrence, severe weather within these environments is much less frequent (Sherburn and Parker 2014; Anderson-Frey et al. 2019). Further, HSLC environments are often coupled with high false alarm rates and low probabilities of detection when severe weather is a threat (Sherburn and Parker 2014; Anderson-Frey et al. 2016, 2019; Sobash and Kain 2017).

There are several different aspects associated with HSLC environments that make forecasting and communicating severe weather challenging. First, the atmosphere typically

rapidly destabilizes prior to severe convection initiation in HSLC environments over small spatial and temporal scales, specifically along and immediately ahead of an advancing cold front in the 3 h preceding severe convection initiation (Sherburn et al. 2016; King et al. 2017). However, operational numerical model forecasts typically only provide hourly output, which is not always sufficient to accurately depict these rapid environmental changes, and the routine observational network is insufficiently dense to reliably detect these changes. Second, severe hazards with HSLC events preferentially occur during the cool season and overnight hours. The public's situational awareness is often low during the cool season, in part owing to the numerous holidays and associated family events that take place during these months (Ashley et al. 2008), and overnight hours, when people are typically sleeping and unable to see ominous conditions or obtain crucial warnings (Paul et al. 2003). Finally, commonly used severe-weather forecasting parameters have limited ability in HSLC environments to effectively quantify a thunderstorm's potential to produce all but the strongest of tornadoes (Guyer and Dean 2010; Thompson 2012; Sherburn and Parker 2014; Anderson-Frey et al. 2019). For example, many of the most frequently used parameters (e.g., Significant Tornado Parameter; Thompson et al. 2003, 2004, 2012; vorticity generation parameter, Rasmussen and Blanchard 1998; and energy helicity index; Davies 1993) were designed with CAPE thresholds above the required thresholds for HSLC environments, limiting their utility for HSLC events.

Several environmental factors are important to severe-weather formation in HSLC environments, including strong synoptic and mesoscale forcing, rapid differences in environmental stability characteristics over small spatial and short temporal scales, and large vertical wind shear magnitude. These events are often associated with strong forcing provided by features such as, but not limited to, upper-level troughs, cold fronts, and surface cyclones (e.g.,

McAvoy et al. 2000; Cope 2004; Lane and Moore 2006; Wasula et al. 2008). Severe convection initiation typically occurs in the warm sector of or along a cold front extending from a midlatitude cyclone in an environment characterized by lower-tropospheric warm, moist air advection and moist planetary boundary layers (Sherburn et al. 2016). While the primary contributor to rapid destabilization is the horizontal advection of warm, moist air originating from the Gulf of Mexico (e.g., Molina and Allen 2019), the release of potential instability through synoptic ascent may also be an important mechanism in some strongly forced HSLC events (King et al. 2017). Furthermore, steep low-level (0-3 km) lapse rates, which can form as a product of strong near-surface warm-air advection and/or surface sensible heating beneath a colder air mass aloft, are also important in HSLC environments. A steeper lapse rate is typically associated with greater buoyancy and correspondingly higher vertical velocity, which leads to enhanced stretching of horizontal vorticity that has been tilted into the vertical by a thunderstorm updraft (Evans and Doswell 2001), and with the generation of more buoyancy-driven turbulence and turbulent eddies that increases downward momentum transport (Parker et al. 2012; Sherburn et al. 2016). Finally, low-level jets (LLJs) that are commonly found in the warm sectors of midlatitude cyclones are associated with intense low-level winds and strong vertical wind shear, with magnitudes of each frequently reaching 25-30 m s^{-1} (Lane and Moore 2006). Strong vertical wind shear is typically also present over deeper vertical layers encompassing much of the troposphere. Strong vertical wind shear often enhances the organization, life cycle, and severity of convection by displacing a thunderstorm's precipitation and outflow from its updraft, promoting mesocyclone formation and persistence in a horizontal-vorticity–rich environment. In short, strong synoptic and mesoscale forcing, along with thermodynamic and kinematic support,

are all important components for the formation of severe weather in HSLC environments and rapid destabilization within these environments.

Short-range convection-allowing model (CAM) forecasts of thunderstorms and their associated hazards in all severe-weather-supporting environments are sensitive to multiple different types of errors and uncertainties, including atmospheric state uncertainty, model error, and land-surface state uncertainty (e.g., Trier et al. 2004, 2011; Melhauser and Zhang 2012; Romine et al. 2013, 2014; Adams-Selin et al. 2013; Schumacher and Clark 2014; Schwartz et al. 2014, 2015; Berner et al. 2015; Cohen et al. 2015; Ha et al. 2015; Lawson and Gallus 2016; Burlingame et al. 2017; Grunzke and Evans 2017; Clark et al. 2018). These sensitivities are well established, but apart from one case-study analysis (Molina et al. 2020), the potential sensitivity of CAM thunderstorm forecasts to the representation of the ocean surface, particularly on synoptic time scales, is less-well-understood. Most CAM forecasts treat the underlying ocean surface as a single layer with a temporally constant sea-surface temperature (SST). By treating the ocean surface in this way, the effects of wind-induced upwelling, the diurnal cycle, and surface heat exchange are not incorporated into the model state, in turn impacting the thermodynamic properties of near-surface air parcels. Furthermore, choices made in constructing SST analyses, such as the assimilation methods used, the data incorporated, whether they represent a skin or foundation temperature, and so on, result in meso- to synoptic-scale SST uncertainties with magnitudes of 0.5-1.0°C (Reynolds and Chelton 2010; Martin et al. 2012; Huang et al. 2021). Differences of this magnitude can influence near-surface stability characteristics in HSLC environments by influencing the magnitude and potentially the direction of the surface sensible and latent heat fluxes that directly influence airmass properties as

inflowing trajectories reach the southeast United States from the Gulf of Mexico, Atlantic Ocean, and/or Caribbean Sea.

While numerous recent studies have advanced our knowledge of HSLC environments and the physical processes resulting in severe weather within these environments, there is still a gap in the knowledge base with regards to how CAMs handle ocean-state uncertainty and the magnitude of the influence this uncertainty might have on severe-thunderstorm predictability in HSLC environments. This research aims to quantify the extent to which short-range CAM forecasts of HSLC severe-weather events are sensitive to the treatment of the underlying ocean surface by testing the hypothesis that explicit severe thunderstorm forecasts are more sensitive to uncertainties in the thermodynamic properties driven by SST uncertainty than to large-scale atmospheric uncertainties. More specifically, when raw CAPE values are low, as in HSLC environments, the impact of small SST uncertainties on air-sea energy exchanges that influence the CAPE of inflowing air parcels are likely to hold a greater potential influence on severe weather potential. The results from this research can inform what types of observations (e.g., those over water and/or near the coastline) are necessary to improve our understanding and predictive ability for cool season severe weather events and inform whether and how ocean-state uncertainty should be represented in NOAA's operational CAMs.

2. Methods

To quantify the impacts of SST uncertainty on cool-season severe weather events, eight HSLC events identified by collaborators from the National Weather Service (NWS) Tallahassee, FL Weather Forecast Office (WFO) are considered for further study. The chosen events posed substantial operational forecast and decision-support challenges to the Tallahassee, FL, Mobile, AL, and/or Slidell, LA WFOs, each of which have forecast and warning responsibilities for

counties along and immediately inland from the northern Gulf of Mexico coastline. A detailed description of the synoptic and mesoscale setup, evolution, and associated hazards for each case is provided in Section 3, whereas a concise description of the eight cases is provided in Table 1.

7 MARCH 2008	A quasi-linear convective system with an embedded line-echo wave pattern signature propagated eastward along the northeastern Gulf of Mexico coastline, resulting in twenty-nine tornado and 37 severe wind reports over the local morning hours (Coleman and Knupp 2010; Ruppert and Bosart 2014).
4 APRIL 2011	A strongly forced squall line propagated eastward through the southeastern United States in conjunction with an advancing cold front, resulting in 68 tornado and over 1,300 severe wind reports. This event served as motivation for revising the definition of a derecho in Corfidi et al. (2016).
25 DECEMBER 2012	A strongly forced squall line propagated eastward through the lower Mississippi Valley in conjunction with an advancing cold front, resulting in 60 tornado and over 100 severe wind reports from eastern Texas to southeast Alabama.
10 FEBRUARY 2013	A quasi-linear convective system propagated eastward across the lower Mississippi Valley ahead of an advancing cold front, resulting in one long-tracked tornado and isolated severe wind reports in southern Mississippi and Alabama (King et al. 2017).
13 OCTOBER 2014	A strongly forced squall line preceded by multiple lines of quasi-discrete supercell thunderstorms propagated eastward across the lower Mississippi Valley ahead of an advancing cold front, resulting in 39 tornado and almost 300 severe wind reports
16-17 NOVEMBER 2014	A squall line preceded by several discrete supercell thunderstorms propagated eastward along the northeastern Gulf of Mexico coastline overnight, resulting in sixteen tornado and 73 severe wind reports between the two days.
2 JANUARY 2017	A bow echo formed and propagated eastward along the northern Gulf of Mexico coastline, resulting in 43 tornado and almost 250 severe wind reports, primarily in central Louisiana, southern Mississippi, southeast Alabama, and southwest Georgia.
21-22 JANUARY 2017	This two-day event exhibited two quasi-linear convective systems propagating eastward across the southeast United States, resulting in over 100 tornado and 300 severe wind reports from far eastern Texas to South Carolina.

Table 1: Summary of the eight HSLC events considered in this study.

Numerical simulations for each of the eight events listed in Table 1 are conducted using version 4.1 of the Advanced Research Weather Research and Forecasting model (WRF-ARW;

Powers et al. 2017; Skamarock et al. 2019). The model configuration closely mimics the operational High-Resolution Rapid Refresh (HRRR; Smith et al. 2008, Benjamin et al. 2016) model often used by forecasters to assist in severe-weather forecasting. The simulation domain, depicted in Figure 1 below, extends from the United States-Canada border southward to the southern extent of the Gulf of Mexico and from the Rocky Mountains eastward to the Gulf Stream.

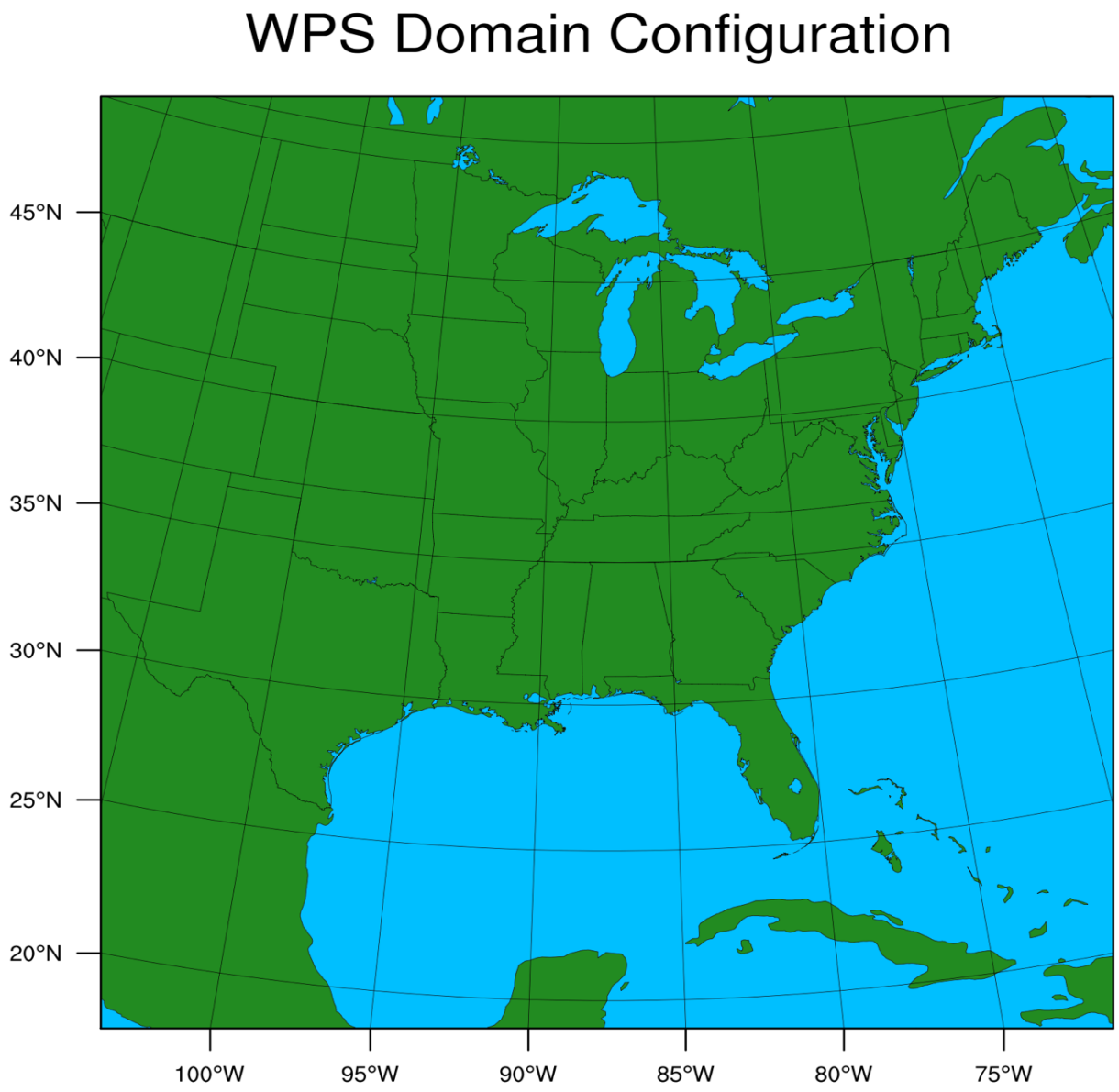

Figure 1: WRF-ARW simulation domain.

The simulations have 3-km horizontal grid spacing and 50 terrain-following vertical levels, ten of which are located within the lowest kilometer above ground level (AGL) to better resolve near-surface kinematic and thermodynamic properties. All simulations are initialized at 0000 UTC on the day on which the severe-weather event begins (except for the cases of 25 December 2012 and 2 January 2017, for which 0600 UTC and 1800 UTC initialization times, respectively, are used to better simulate the evolution of the observed severe-weather event). Simulations extend forward for 36 h except for the 16-17 November 2014, 2 January 2017, and 21 January 2017 cases, which extend forward 48 h, 42 h, and 48 h, respectively, to ensure the entirety of the severe-weather event is captured by the simulation. Initial and lateral boundary conditions for the model simulations are provided by the 12-km North American Mesoscale (NAM; Janjić 2013) model analysis and forecast from the forecast cycle corresponding to the simulation initialization time. A full list of model configurations and physical parameterizations is provided in Table 2.

WRF-ARW v4.1 Specifications		**References**
Horizontal Grid Spacing	3 km	
Vertical Grid Spacing	50 terrain-following Levels	
Initial & Lateral Boundary Conditions for the SST Sensitivity Simulations	12 km North American Mesoscale Model	Janjić (2013)
Initial & Lateral Boundary Conditions for the SST vs. Atmospheric Sensitivity Simulations	European Center for Medium-Range Weather Forecasts Reanalysis 5th Generation 10-Member Ensemble Reanalysis	Hersbach et al. (2020)
Planetary Boundary & Surface Layer	Mellor-Yamada-Nakanishi-Niino Level 2.5	Nakanishi and Niino (2006)
Microphysics	Thompson	Thompson et al. (2008)
Shortwave and Longwave Radiation	Rapid Radiative Transfer Model for General Circulation Models	Iacono et al. (2008)
Land-Surface Model	Noah	Chen and Dudhia (2001)

Table 2: WRF-ARW simulation configuration details.

a. SST Sensitivity Method

This study uses two complementary approaches to investigate the influence of ocean-state uncertainty in CAMs on severe-weather forecasts. In the first, a six-member ensemble of forecasts is conducted for each case, with each ensemble member varying only by the SST analysis used to represent the oceanic state in each forecast. Since most widely available SST analyses only update daily, SSTs in each model simulation are held fixed at their values at the model initialization time for each case. The control simulation represents SSTs using the SST analysis provided with the NAM analyses. The SSTs in the remaining five ensemble members are represented using the Remote Sensing Systems Microwave Optimal Interpolation v5.0 (REMSS 2021), the Group for High-Resolution Sea-Surface Temperature Level 4 Multiscale Ultra-high Resolution Sea-Surface Temperature (GHRSST; Chin et al. 2017), the US Navy Fleet Numerical Meteorology and Oceanography Center High-Resolution Sea-Surface Temperature (FNMOC; Donlon et al. 2007), the US Naval Oceanographic Office Global Hybrid Coordinate Ocean Model (USNO; Cummings and Smedstad 2013; Metzger et al. 2014), or the NOAA Optimum Interpolation v2 Sea-Surface Temperature (NOAAOI; Reynolds et al. 2007, 2013) SST analyses. Brief descriptions of these SST datasets are found in Table 3. It is important to keep in mind that without a fully coupled ocean-atmosphere model and/or prescribed time-varying SSTs, the effects of the diurnal cycle and wind-induced vertical mixing cannot be represented and are not represented in these simulations. However, variations in SST analysis input data and generation methods that are captured by the ensemble provide a reasonable estimate of the overall SST uncertainty associated with each event in the absence of a fully coupled model.

Sea-Surface Temperature Analysis Specifications				
Analyses	**Horizontal Grid Spacing**	**Temporal Frequency**	**General Description**	**Reference**
Remote Sensing Systems Microwave Optimal Interpolation (REMSS)	0.25°	Daily	Combines through-cloud microwave data with infrared data, adjusted using a diurnal model.	Remote Sensing Systems (www.remss.com)
Group for High-Resolution Sea-Surface Temperature Level 4 Multiscale Ultra-high Resolution Sea-Surface Temperature (GHRSST)	0.011°	Daily	Uses a multi-resolution variational analysis procedure used to combine ship, buoy, float, and satellite-derived SST and sea-ice data from infrared and microwave imagers.	Chin et al. (2017)
US Navy Fleet Numerical Meteorology and Oceanography Center High-Resolution Sea-Surface Temperature (FNMOC)	0.081°-0.109°	Daily	Combines satellite-derived, ship, and buoy SST and sea-ice concentration observations.	Donlon et al. (2007)
US Naval Oceanographic Office Global Hybrid Coordinate Ocean Model (USNO)	0.083°	Daily	Three-dimensional variational analysis used to combine ship, buoy, float, bathythermograph, and satellite-derived SST and sea-ice data.	Cummings and Smedstad 2013, Metzger et al. 2014
NOAA Optimum Interpolation v2 Sea-Surface Temperature (NOAAOI)	0.25°	Daily	Combines bias-corrected satellite-derived AVHRR SST retrievals, sea ice concentrations, and ship and buoy data.	Reynolds et al. (2007, 2013)

Fifth-generation ECMWF (ERA5) - Post-August 2007: Met Office Operational SST and Sea Ice Analysis (OSTIA)	0.05°	Daily	Combines data from in-situ instruments, microwave imagers, and geostationary satellites.	Donlon et al. (2012), Hirahara et al. (2016)
North American Mesoscale (NAM): NCEP RTG_SST_HR	0.125°	Daily	Combines bias-corrected satellite-derived SST retrievals, buoy, ship, and sea ice concentration data.	Janjić (2013)

Table 3: SST analysis descriptions and specifications

b. SST vs. Atmospheric Sensitivity Method

The first set of ensemble forecasts intends to quantify the influence of oceanic-state uncertainty on eight HSLC severe-weather events but is unable to compare this influence to that from initial atmospheric uncertainty. This motivates the second approach used in this study. This approach consists of a 60-member ensemble of forecasts that includes both SST and atmospheric uncertainty for one selected case event, 13 October 2014, with the subjectively largest SST ensemble variability. Additionally, the results of the calculated root mean difference total energy (RM-DTE; see sections 3c and 4) provide support for the choice of this case. For this case, the fifth-generation ECMWF ERA5 (Hersbach et al. 2020) ten-member ensemble reanalysis is used to initialize and provide lateral boundary conditions for the WRF-ARW model forecasts. Each ensemble reanalysis condition is paired with each of the non-NAM SST datasets listed in Table 3 to generate the 60-member ensemble. The model configuration is otherwise identical to that described earlier and documented in Table 2. This approach allows us to quantify the forecast sensitivities for this case resulting from SST uncertainty alone (across the SST analyses for each ensemble reanalysis member) and atmospheric uncertainty alone (across the ensemble reanalysis

for each SST analysis), ultimately allowing for preliminary conclusions to be drawn regarding the magnitude of the potential influence of ocean-state uncertainties on CAM forecasts for HSLC severe-weather events.

c. Verification Data and Methods

The influences of SST and initial atmospheric uncertainty on forecast variability are quantified by using the enhanced Model Evaluation Tools (Brown et al. 2021) package to verify each ensemble member's model-forecast 2-5 km AGL updraft helicity (UH) swaths against preliminary Storm Prediction Center local storm reports (LSRs) using neighborhood verification methods. The forecast skill variability across the ensemble is then used as a proxy for the influence of SST and/or initial atmospheric uncertainty on the more-general forecast variability.

UH is utilized both operationally and for research purposes as a supercell and severe-weather proxy. These uses include, but are not limited to, using UH as surrogates for severe-weather occurrences and verifying CAMs (Kain et al. 2008; Sobash et al. 2016; Sobash and Kain 2017; Gallo et al. 2019; Roberts et al. 2020). UH is defined as:

$$UH = \int_{z1}^{z2} \boldsymbol{w\zeta dz}$$

where z1 and z2 are the layer which UH is calculated (here being 2-5 km AGL), w is the vertical velocity, and ζ is vertical vorticity. A variety of UH thresholds are used to create the surrogates for verification purposes following the procedures used in past studies focused on model verification (Sobash and Kain 2016, 2017). These thresholds are 10.1 $m^{-2}s^{-2}$, 33.4 $m^{-2}s^{-2}$, 45.7 $m^{-2}s^{-2}$, and 78.6 $m^{-2}s^{-2}$, which correspond to the 95th, 99th, 99.5th, and 99.9th percentile values of the UH distributions for all control simulations of the eight cases considered in this study. The UH is regridded onto a roughly 80 km x 80 km grid in which the maximum UH value within 80 km is applied to grid point, which is consistent with the grid used by the SPC for probabilistic

outlooks and subsequent forecast verification, and a binary grid is created where all grid cells are equal to zero if the specified UH threshold is not reached and one if the specified UH threshold is reached.

A neighborhood verification approach is chosen to determine the general impact of SST uncertainty in forecasts. Using a neighborhood approach accounts for discrepancies in the location and timing of modeled severe-weather surrogates and LSRs. Forecasts are verified using LSRs, including observed tornadoes, severe hail (greater than 19.05 mm for 7 March 2008 and 25.4 mm for all other cases, consistent with then-current operational severe thresholds), and severe wind (10-m wind speeds more than 25.93 m s^{-1} and/or damage caused by thunderstorm winds). The LSRs are mapped onto an 80 km x 80 km grid (matching that of the regridded model data) as a binary field, where a value of 1 is given to grid cells containing at least one LSR and a value of 0 is given to grid cells containing no LSRs. The gridding process used here helps to reduce negative impacts from population density, such as overreporting biases, that are a known pitfall of using LSRs as a verification dataset (Weiss and Vescio 1998; Verbout et al. 2006; Cintineo et al. 2012), by filtering out these biases using the relatively coarse grid. Specifically, in areas where the population density is great, like in much of the southeastern United States, there is evidence that overreporting biases can influence the number of LSRs that occur for any given severe weather event. In addition, inconsistencies in reporting practices between different WFOs can lead to a level of added uncertainty in results when using LSRs in verification. While the negative qualities of using LSRs are important to keep in mind, using LSRs is a common practice in verification methods of CAMs.

Forecast verification is performed using the fractions skill score (FSS; Roberts and Lean 2008). FSS is calculated following Roberts and Lean (2008) as:

$$\mathrm{FSS} = 1 - \frac{\mathrm{FBS}}{\frac{1}{N}\left[\sum_N \langle P_f \rangle_s^2 + \sum_N \langle P_o \rangle_s^2\right]}$$

where the fractions Brier score, or FBS, is calculated as:

$$\mathrm{FBS} = \frac{1}{N}\sum_N [\langle P_f \rangle_s - \langle P_o \rangle_s]^2$$

P_{fs} is the proportion of grid boxes within a forecast neighborhood where the threshold is exceeded, and P_{os} is the proportion of grid boxes within the observed neighborhood where the threshold is exceeded (in this case a value of 1 since a binary grid is used in place of thresholds). The FSS is used to measure the agreement in the fractional coverage of modeled and observed quantities within a given neighborhood. Two circular neighborhood sizes are used in this study to compute the FSS, a 9-point neighborhood with a is ~120 km radius and a 25-point neighborhood with a ~ 200 km radius. The FSS is computed over the 24-h period in which the observed severe-weather reports occurred for each case except for 21-22 January 2017, for which FSS is computed only for the second of two separate severe-weather events.

To further investigate the effects of SST and initial atmospheric uncertainty on short-range forecast spread, RM-DTE is computed for the SST sensitivity ensembles per case and with the SST versus atmospheric sensitivity simulations, creating ensembles holding the SST constant with varying atmospheric conditions and also ensembles holding the atmospheric conditions constant with varying SSTs. The form of RM-DTE used in this study follows that of several past studies and provides insight into the magnitude and spatial distribution of an ensemble's spread (e.g., Mitchell et al. 2002; Zhang et al. 2006; Meng and Zhang 2007; Sippel and Zhang 2008). The DTE is calculated as:

$$DTE = 0.5(u'u' + v'v' + kT'T')$$

where the prime quantities refer to the difference between a member and the ensemble mean, u and v are the zonal and meridional velocities, $k = C_p/T_r$ where C_p = 1004.9 J kg^{-1} K^{-1} and the reference temperature T_r = 270 K, and T is the temperature. The RM-DTE is the square root of the ensemble- and vertically averaged DTE. For this study, DTE is vertically averaged over the lowest 14 terrain-following model levels, which correspond to sigma = 0.999 to sigma = 0.706 (or from the surface to approximately 700 hPa) for the simulations conducted herein. This method is used to emphasize contributions of SST uncertainty (most likely influencing near-surface properties) to atmospheric variability in the lower troposphere and it differs from past studies that typically integrate over all levels.

3. Cases Considered

a. 7 March 2008

The 0000 UTC 7 March 2008 250-hPa analysis indicates a trough extending from Canada to western Texas through the west-central United States. By 0000 UTC 8 March 2008, the trough is associated with a southwest-to-northeast oriented jet streak located to the east of the base of the trough, with peak wind speeds between 125-150 kt, located over the Gulf of Mexico just off the coast of Texas and Louisiana. The 0000-1200 UTC 7 March 2008 850 hPa analyses (e.g., Fig. 2b) indicates the formation of a lower-tropospheric cyclone over the coastal region of the southeast United States. A warm and moist lower-tropospheric air mass is present across the far southeast United States ahead of an advancing cold front associated with the developing lower-tropospheric cyclone. Surface analysis (e.g., Fig. 2c) indicates the development of a weak (minimum sea-level pressure of approximately 1004 hPa) low-pressure system over New Orleans, LA at 0600 UTC 7 March 2008. This low-pressure system propagates to the east along the northern Gulf Coast from 0600-1200 UTC before moving inland after reaching the Florida

panhandle. SSTs in the Gulf of Mexico are approximately 16°C along much of the coast, with temperatures reaching 26-28°C in the central Gulf (e.g., Fig 2d). The Storm Prediction Center's (SPC) 1200 UTC 7 March 2008 Day 1 Convective Outlook (e.g., Fig 2e) places most of Florida, southern Georgia, and the eastern portions of the Carolinas under a slight risk for severe weather, with the potential for a few tornadoes, large hail, and damaging winds (NOAA 2008). The thunderstorm evolution with this event is characterized by the formation of a quasi-linear convective system (QLCS), in which embedded line-echo wave pattern signatures are detected via radar imagery. This event is associated with twenty-nine tornado reports, five hail reports, and 37 severe wind reports primarily throughout Florida and Georgia (NOAA 2008; Fig. 2f).

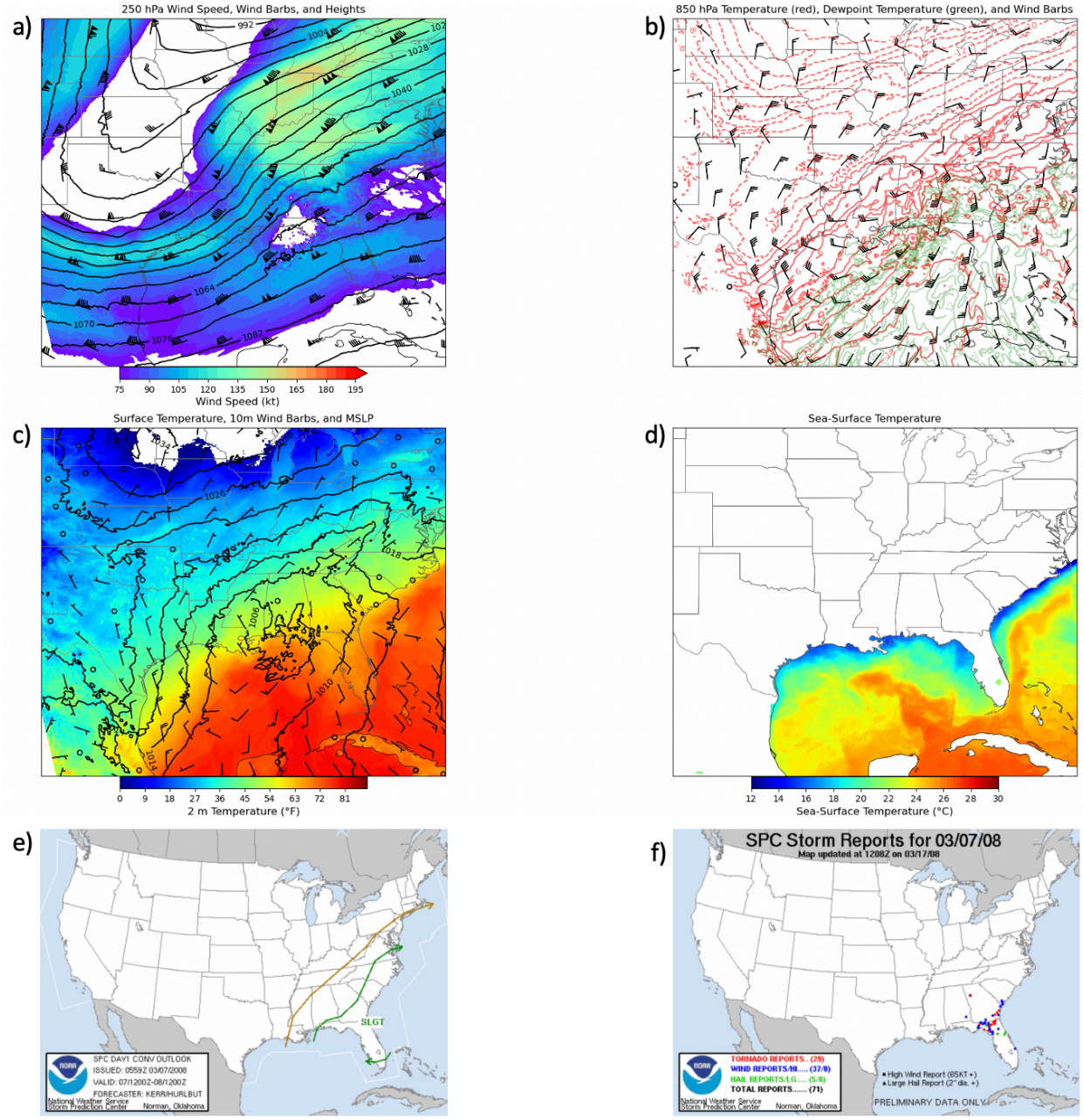

Figure 2: 1200 UTC 7 March 2008 analyses for: a) 250 hPa shaded wind speeds (kt), wind barbs (half-barb = 5 kt, full barb = 10 kt, pennant = 50 kt), and height contours (dm), b) 850 hPa temperature contours (red; °C), dewpoint temperature contours >8°C (green; °C), and height contours (dm), c) shaded surface temperature (°F), 10-m wind barbs (half-barb = 5 kt, full barb = 10 kt, pennant = 50 kt), and mean sea-level pressure contours (hPa), d) shaded SST (°C), e) SPC Day 1 Convective Outlook (contours) obtained by NOAA/NWS Storm Prediction Center, and f) Local Storm Reports (red=tornado, green=hail, blue=wind) obtained by NOAA/NWS Storm Prediction Center.

b. 4 April 2011

The 0000 UTC 4 April 2011 250 hPa analysis depicts the southeastern United States situated under a ridge, with a trough located to the west over the Rocky Mountains. By 0000 UTC 5 April 2011, this trough deepens and moves eastward into the east-central United States, with the right-entrance region of a jet streak located north of the eastern side of the trough over the Mississippi River valley and the jet streak itself (with maximum wind speeds between 175-200 kt) centered over the Great Lakes. At 850 hPa (e.g., Fig. 3b), at 0000 UTC 4 April 2011, an area of low-pressure is centered over Minnesota and Wisconsin, with a southwest trailing cold front. Ahead of the cold front, dewpoint temperatures greater than 10°C are present within southerly flow throughout Texas and Louisiana. Over the next 24 h, this area of low-pressure propagates to the northeast with the cold front propagating through the Mississippi River valley. The trend of high dewpoint values aided by southwesterly flow on the lee side of the trough continues. The 850 hPa analyses also indicate the presence of a LLJ, with maximum wind speeds reaching 60 kt, ahead of the cold front. Surface analysis indicates a low-pressure centered over Iowa at 0000 UTC 4 April 2011 that moves to the northeast. By 1200 UTC 4 April 2011 (e.g., Fig. 3c), the low is centered over Michigan, with a strong cold front (evident via sharp temperature gradients and strong winds) extending from Michigan southwestward to Texas. Gulf of Mexico SSTs are approximately 21-23°C along much of the coast, with slightly warmer temperatures near 25°C off the Louisiana coast. Temperatures near the middle of the Gulf reach about 27°C (e.g., Fig 3d). The 1200 UTC Day 1 Convective Outlook (e.g., Fig. 3e) produced by the SPC includes a moderate risk area over western Tennessee and the northern half of Mississippi (NOAA 2011). SPC forecasters warn of an enhanced threat of damaging winds due to strong deep layer shear associated with strong lower- and mid-tropospheric jets. In addition to

the wind threat, a risk of embedded tornadoes within the forecasted QLCS and large hail within any intense cores are also highlighted as threats with this event. This case is characterized by the formation of a strongly forced QLCS that is coupled with the advancing cold front previously analyzed. The event results in severe reports throughout a large area of the southeast United States, including 68 tornado reports, 90 hail reports, and over 1,300 severe wind reports (NOAA 2011; Fig. 3f).

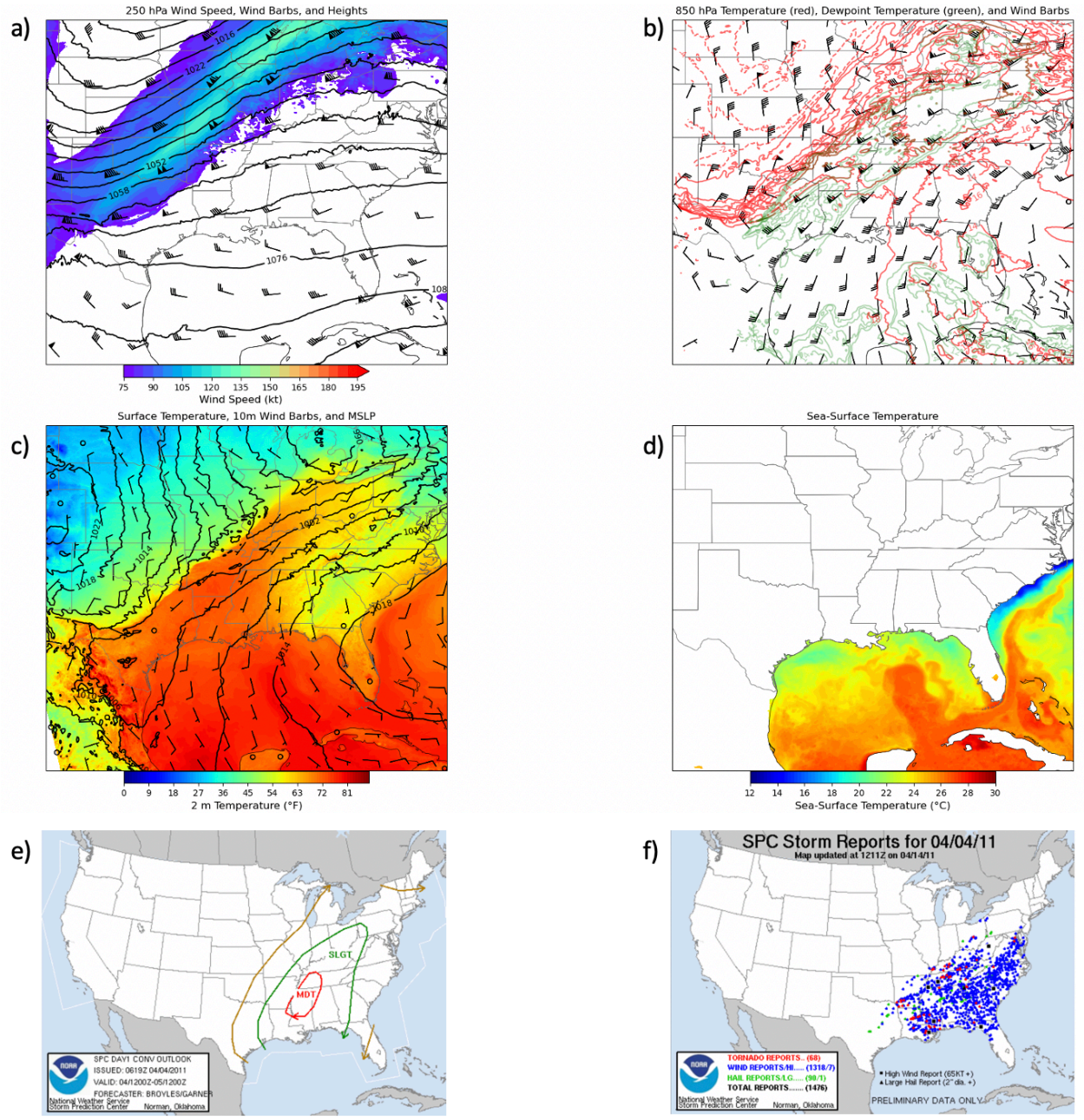

Figure 3: 1200 UTC 4 April 2011 analyses for: a) 250 hPa shaded wind speeds (kt), wind barbs (half-barb = 5 kt, full barb = 10 kt, pennant = 50 kt), and height contours (dm), b) 850 hPa temperature contours (red; °C), dewpoint temperature contours >8°C (green; °C), and height contours (dm), c) shaded surface temperature (°F), 10-m wind barbs (half-barb = 5 kt, full barb = 10 kt, pennant = 50 kt), and mean sea-level pressure contours (hPa), d) shaded SST (°C), e) SPC Day 1 Convective Outlook (contours) obtained by NOAA/NWS Storm Prediction Center, and f) Local Storm Reports (red=tornado, green=hail, blue=wind) obtained by NOAA/NWS Storm Prediction Center.

c. 25 December 2012

Upper-air analysis (e.g., Fig 4a) of this event indicates a developing jet streak to the west of the base of a trough at 250 hPa with wind speeds up to 150 kts over western Texas from 1200 UTC 25 December 2012 to 0000 UTC 26 December 2012. This upper-level jet streak, coupled with a shortwave trough, amplifies as they moved eastward throughout the day, becoming more negatively tilted and positioned over the Midwest by 1200 UTC 26 December 2012. 850 hPa analyses (e.g., Fig. 4b) indicates the development of a lower-tropospheric low-pressure system over central Texas at 1200 UTC 25 December 2012 that propagates to the east-northeast through 1200 UTC 26 December 2012. Southwesterly wind speeds near the Gulf Coast on the eastern portion of this low-pressure exceeds 50 kt by 0000 UTC 26 December 2012. A surface low-pressure system develops in eastern Texas between 1200-1800 UTC 25 December 2012 (e.g., Fig 4c) and continuously deepens as it propagates to the northeast and into Tennessee by 1200 UTC 26 December 2012. As the associated cold front advances east, the airmass ahead of the front increases in moisture, with dewpoint temperatures reaching 16-18°C. SSTs along the Gulf coast are approximately 18-22°C, while temperatures near the center of the Gulf reach approximately 28°C (e.g., Fig 4d). The SPC Day 1 Convective Outlook (e.g., Fig. 4e) for this case consists of a moderate risk throughout portions of far eastern Texas, southern Louisiana, southern Mississippi, and southwestern Alabama (NOAA 2012). The SPC cautions for the chance of a few strong and potentially long-lived tornadoes with this system, owing to model guidance showing evidence of deep layer shear development that would be supportive of rotating supercells. Radar analysis indicates supercell development by 0700 UTC 25 December 2012 throughout eastern Texas and Louisiana; however, most severe reports from this case occur after the storms grow upscale into a QLCS, around 1700 UTC. This event is responsible for 60

tornado reports, three severe hail reports, and over 100 severe wind reports across the Gulf Coast states (NOAA 2012; Fig. 4f).

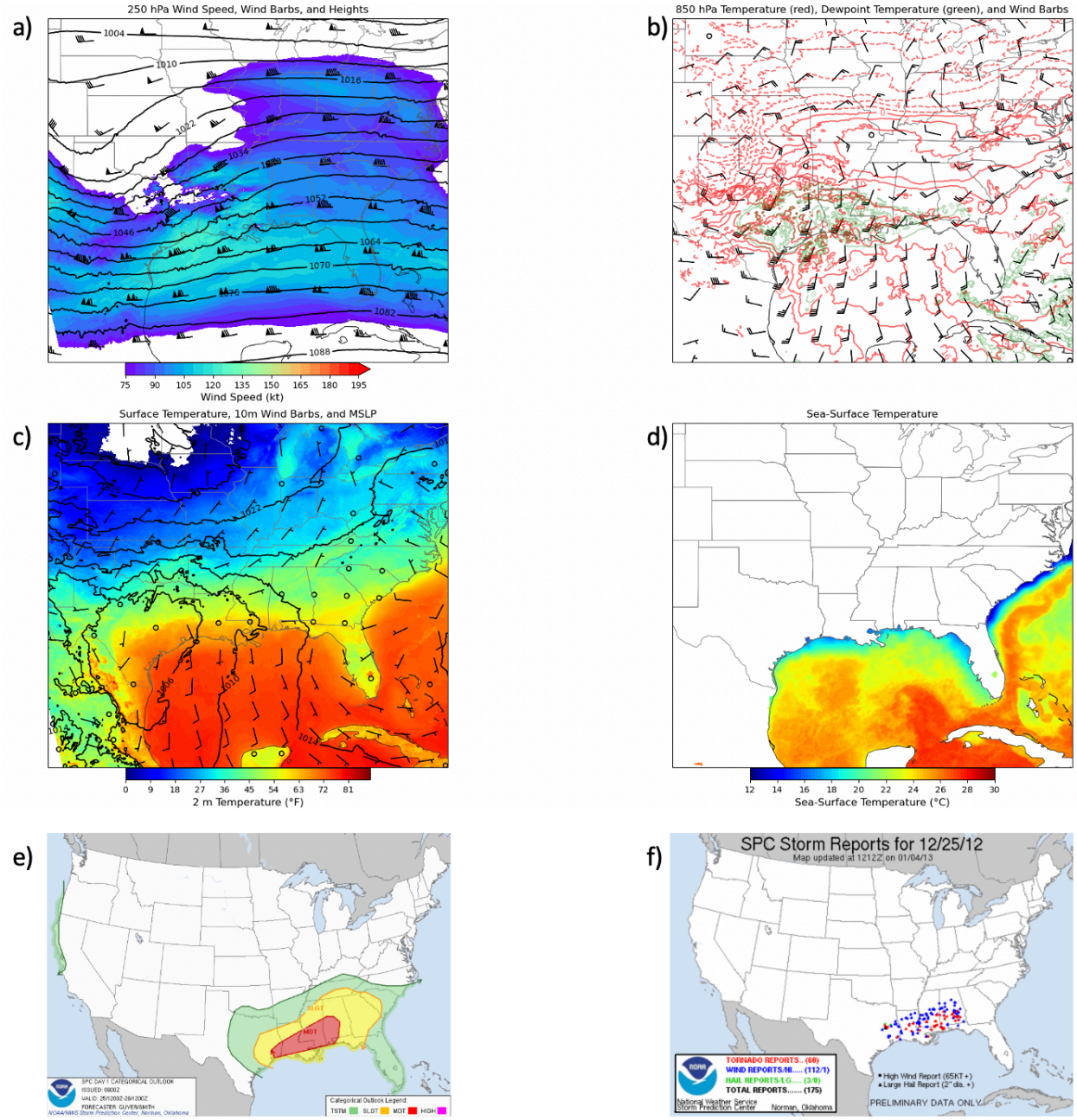

Figure 4: 1200 UTC 25 December 2012 analyses for: a) 250 hPa shaded wind speeds (kt), wind barbs (half-barb = 5 kt, full barb = 10 kt, pennant = 50 kt), and height contours (dm), b) 850 hPa temperature contours (red; °C), dewpoint temperature contours >8°C (green; °C), and height contours (dm), c) shaded surface temperature (°F), 10-m wind barbs (half-barb = 5 kt, full barb = 10 kt, pennant = 50 kt), and mean sea-level pressure contours (hPa), d) shaded SST (°C), e) SPC Day 1 Convective Outlook (contours) obtained by

NOAA/NWS Storm Prediction Center, and f) Local Storm Reports (red=tornado, green=hail, blue=wind) obtained by NOAA/NWS Storm Prediction Center.

d. 10 February 2013

This event is primarily characterized by marginal instability compared to the previously discussed cases. 250 hPa analysis (e.g., Fig. 5a) indicates a trough extending from Canada southward through the western United States from 0000 UTC 10 February 2013 through 1200 UTC 11 February 2013. Near the base of the trough, a developing jet streak over Texas is also evident, with wind speeds reaching up to 175 kt, from 0000 UTC 10 February 2013 to 0000 UTC 11 February 2013. This event differs from others in that there is no trough actively propagating through the central and eastern United States at 250 hPa, leaving these areas under a primarily southwesterly flow at this level. A low-pressure system is located at the 850 hPa level over Nebraska at 1200 UTC 10 February 2013 (e.g., Fig. 5b), with indications of a moist airmass over the southern Gulf states evidenced by dewpoint temperatures greater than 12°C. At the surface, 1200 UTC analysis on 10 February 2013 (e.g., Fig. 5c) indicates a low-pressure center over Nebraska, with a cold front draped through eastern Kansas, Oklahoma, and Texas and a warm front extending out ahead of the cold front. As the low-pressure system moves northeastward the surface dewpoint temperatures reach 16-18°C within the warm sector. Gulf of Mexico SSTs along the coast are approximately 17-22°C. Temperatures near the center of the Gulf reach approximately 26-28°C, with only a narrow north-to-south oriented area reaching the maximum temperatures (e.g., Fig 5d). The 1200 UTC SPC Day 1 Convective Outlook (e.g., Fig. 5e) indicates a slight risk over the Mississippi River valley, with forecasters citing marginal instability due to weak lapse rates. However, a favorable shear environmental setup courtesy of strong veering of the winds with height is the reasoning for the categorical risk associated with this event and the SPC warns for the potential for locally damaging winds and a few isolated

tornadoes (NOAA 2013). The thunderstorm evolution for this event is characterized by an eastward propagating sub-severe QLCS until about 1800 UTC 10 February 2013, when storms began to initiate ahead of the advancing cold front. After 1800 UTC, radar analysis indicates more discrete cells, that are responsible for producing severe weather, and a less organized linear structure to the storms. This case consists of nineteen tornado reports, eleven hail reports, and 34 severe wind reports (NOAA 2013; Fig. 5f).

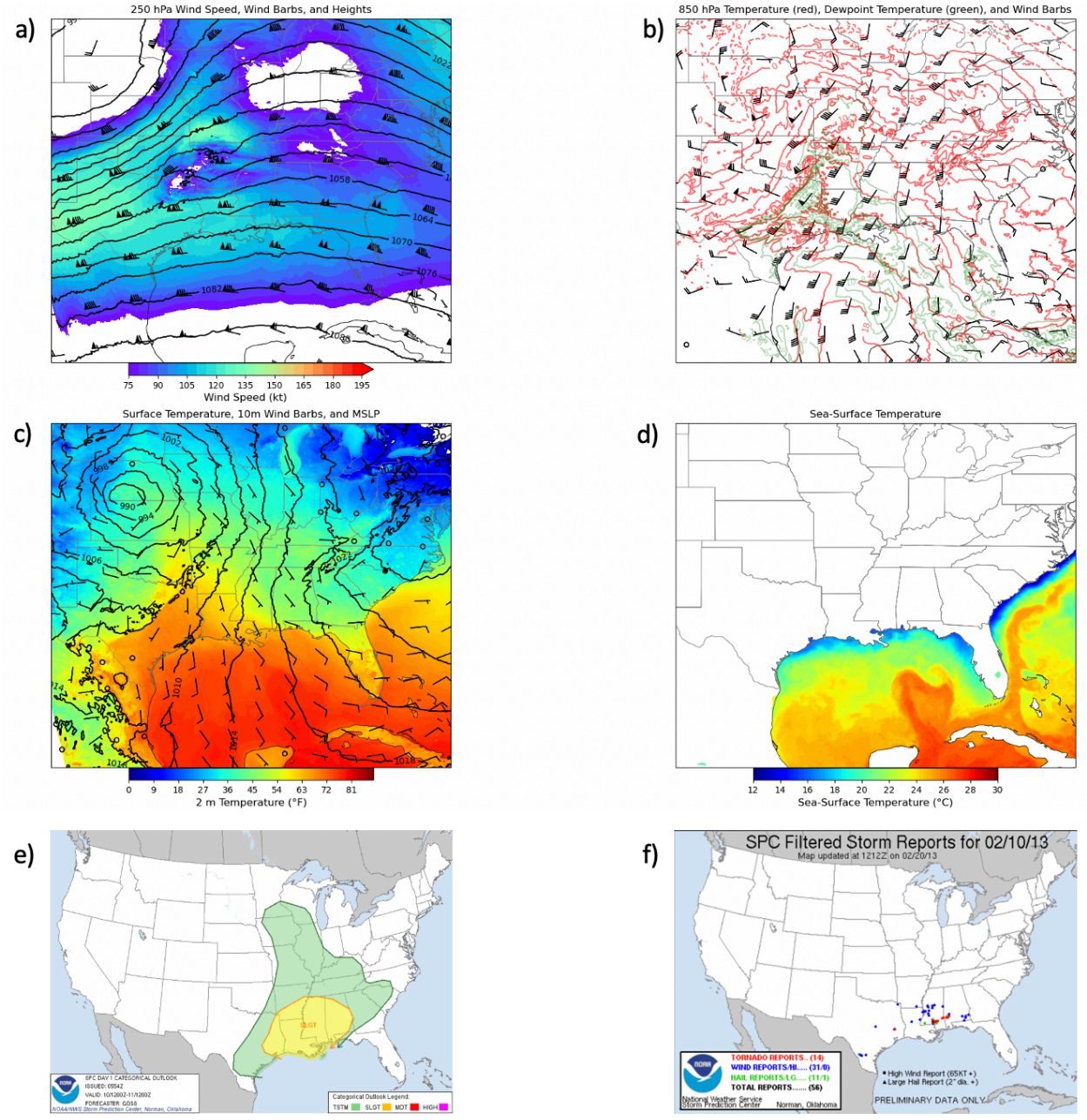

Figure 5: 1200 UTC 10 February 2013 analyses for: a) 250 hPa shaded wind speeds (kt), wind barbs (half-barb = 5 kt, full barb = 10 kt, pennant = 50 kt), and height contours (dm), b) 850 hPa temperature contours (red; °C), dewpoint temperature contours >8°C (green; °C), and height contours (dm), c) shaded surface temperature (°F), 10-m wind barbs (half-barb = 5 kt, full barb = 10 kt, pennant = 50 kt), and mean sea-level pressure contours (hPa), d) shaded SST (°C), e) SPC Day 1 Convective Outlook (contours) obtained by NOAA/NWS Storm Prediction Center, and f) Local Storm Reports (red=tornado, green=hail, blue=wind) obtained by NOAA/NWS Storm Prediction Center.

e. 13 October 2014

Upper-air analysis at 250 hPa (e.g., Fig. 6a) indicates a trough that deepens as it propagates eastward from the lee side of the Rocky Mountains into the central United States. 850 hPa analysis (e.g., Fig. 6b) indicates a moist environment to the east of the trough axis, with dewpoint temperatures reaching up to 16°C. A well-developed LLJ is also present with wind speeds greater than 50 kt over portions of the Mississippi River valley from 1200 UTC 13 October 2014 to 0000 UTC 14 October 2014. 0000 UTC 13 October 2014 surface analysis shows a low-pressure system located over the eastern portion of Oklahoma's panhandle. The cold front associated with this low moves swiftly eastward and is located through Texas and portions of Arkansas by 1200 UTC 13 October 2014 (e.g., Fig. 6c), with the low in central Oklahoma. Dewpoint temperatures ahead of the cold front reach between 20-22°C well inland from the Gulf of Mexico, indicating a moisture rich environment. This case stands separate from the others considered in this study when analyzing the Gulf of Mexico SSTs (e.g., Fig 6d), for which this case exhibits much warmer temperatures than all other cases. The SSTs are approximately 30°C throughout the entirety of the Gulf, with slightly cooler (~28°C) temperatures along the coast. The SPC indicates a moderate risk for severe weather centered along the Mississippi river from Louisiana to the Illinois border with their 1200 UTC Day 1 Convective Outlook (e.g., Fig. 6e), with the largest threat being widespread wind damage (NOAA 2014). This case is characterized by a QLCS associated with the advancing cold front, with several quasi-discrete supercells that form within the warm sector of the system. Overall, this event produces 39 tornado reports, 23 severe hail reports, and 291 wind reports ranging from the Gulf Coast to central Illinois (NOAA 2014; Fig. 6f).

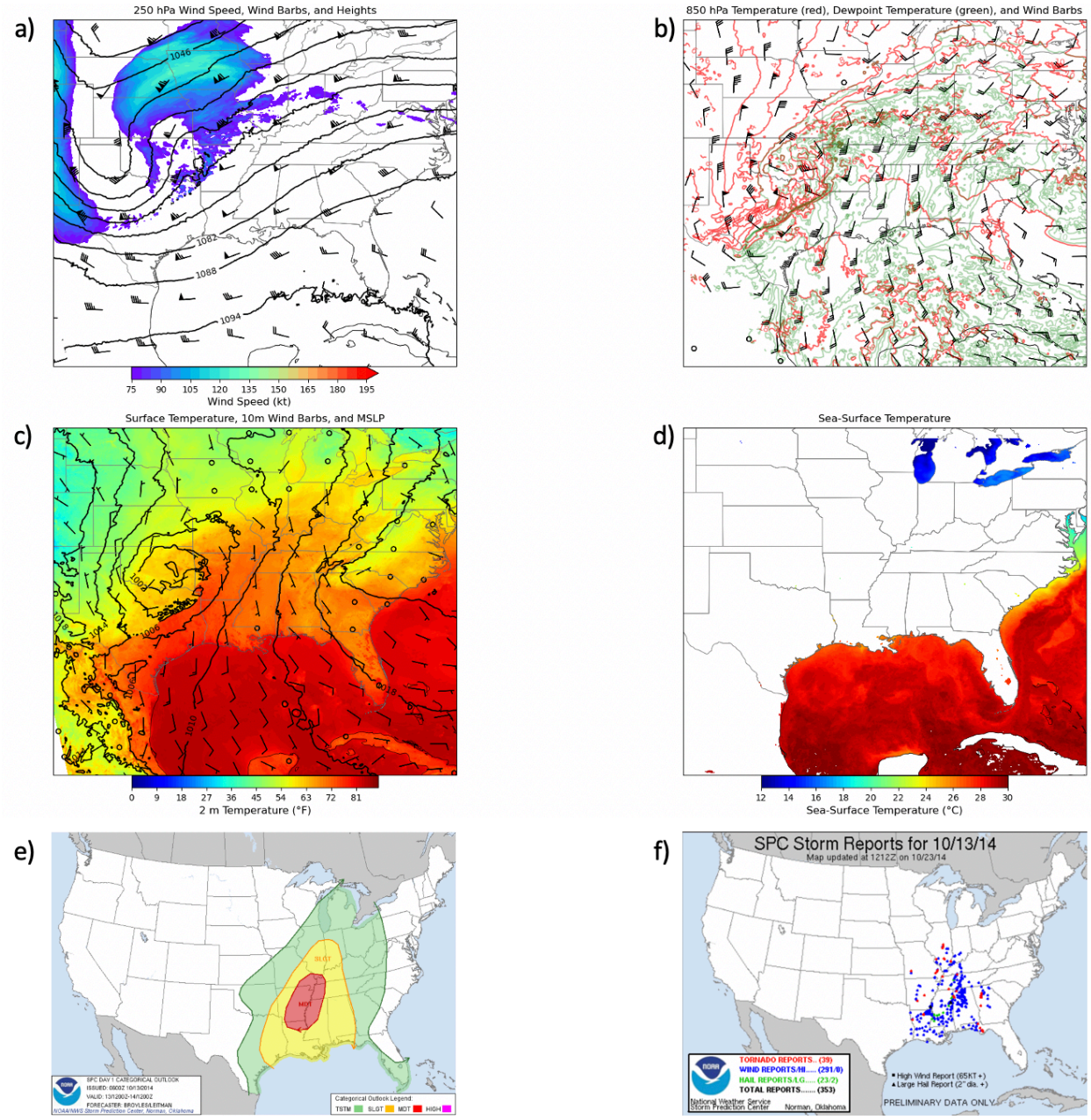

Figure 6: 1200 UTC 13 October 2014 analyses for: a) 250 hPa shaded wind speeds (kt), wind barbs (half-barb = 5 kt, full barb = 10 kt, pennant = 50 kt), and height contours (dm), b) 850 hPa temperature contours (red; °C), dewpoint temperature contours >8°C (green; °C), and height contours (dm), c) shaded surface temperature (°F), 10-m wind barbs (half-barb = 5 kt, full barb = 10 kt, pennant = 50 kt), and mean sea-level pressure contours (hPa), d) shaded SST (°C), e) SPC Day 1 Convective Outlook (contours) obtained by NOAA/NWS Storm Prediction Center, and f) Local Storm Reports (red=tornado, green=hail, blue=wind) obtained by NOAA/NWS Storm Prediction Center.

f. 16-17 November 2014

This two-day case event's upper-air analysis progression exhibits a trough throughout the Great Plains and the development of a jet streak to the northeast of the base of the trough from 1200 UTC 16 November 2014 (e.g., Fig. 7a) to 1200 UTC 17 November 2014, with maximum wind speeds reaching between 200-225 kt at the core of the jet located over the Great Lakes. Evidence of an eastward propagating shortwave trough is seen when analyzing the 850 hPa level charts (e.g., Fig. 7b), and it is this shortwave feature that leads to enhancement of the risk for severe weather in this case. Surface analysis (e.g., Fig. 7c) indicates the presence of a low-pressure system and associated cold front positioned over southwest Mississippi at 0000 UTC 17 November 2014 that propagates to the northeast into North Carolina by 1800 UTC 17 November 2014. The severe weather associated with this event takes place after 2300 UTC 16 November 2014 and continues throughout the night until about 1800 UTC 17 November 2014. SSTs located in the Gulf of Mexico, along the coast, are variable, with temperatures ranging from approximately 16-23°C. Temperatures throughout much of the center of the Gulf are approximately 26-28°C, with some areas near the southern extent reaching almost 30°C (e.g., Fig 7d). The SPC's Day 1 Convective Outlook for 1200 UTC 16 November 2014 (e.g., Fig. 7e) consists of a small area covering southern Louisiana, Mississippi, and Alabama placed under a slight risk for severe weather, with the associated risks being primarily a tornado threat with isolated wind damage and marginally severe hail (NOAA 2014). The 1200 UTC SPC Day 1 Convective Outlook for 17 November 2014 shifts the area of risk to be centered over northern Florida, southeastern Georgia, and coastal South Carolina, again with the categorical risk being considered slight. The primary risk on this second day of severe weather iss isolated damaging winds. This event's thunderstorm evolution is characterized by an initial QLCS along the cold

front and discrete supercells that begin to form around 0900 UTC 17 November 2014 in the warm sector ahead of the cold front, which become more linear in structure as they propagate eastward throughout Georgia. By 1900 UTC 17 November 2014 the storms move along the Atlantic coast, with only the Florida panhandle still experiencing thunderstorms. Throughout this two-day event, a total of sixteen tornadoes and 73 severe wind reports were recorded (NOAA 2014; Fig. 7f).

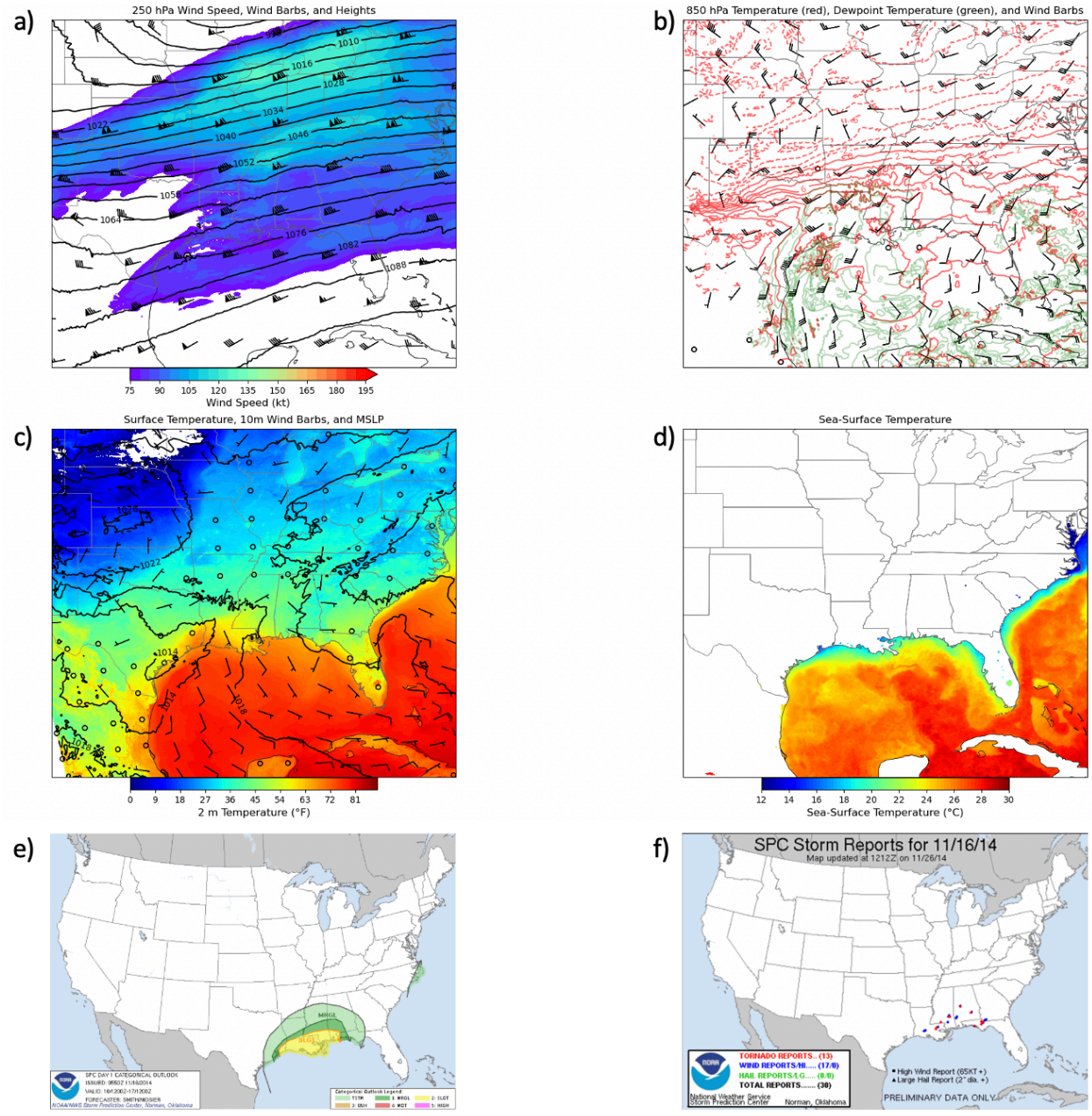

Figure 7: 1200 UTC 16 November 2014 analyses for: a) 250 hPa shaded wind speeds (kt), wind barbs (half-barb = 5 kt, full barb = 10 kt, pennant = 50 kt), and height contours (dm), b) 850 hPa temperature contours (red; °C), dewpoint temperature contours >8°C (green; °C), and height contours (dm), c) shaded surface temperature (°F), 10-m wind barbs (half-barb = 5 kt, full barb = 10 kt, pennant = 50 kt), and mean sea-level pressure contours (hPa), d) shaded SST (°C), e) SPC Day 1 Convective Outlook (contours) obtained by NOAA/NWS Storm Prediction Center, and f) Local Storm Reports (red=tornado, green=hail, blue=wind) obtained by NOAA/NWS Storm Prediction Center.

g. 2 January 2017

Upper-air analysis for this case depicts a shortwave trough at 250 hPa (e.g., Fig. 8a) propagating eastward from the Rocky Mountains to the Midwest from 0000 UTC 2 January 2017 to 0000 UTC 3 January 2017, with increasingly zonal flow behind the trough. A surface low is evident over eastern Texas by 1200 UTC 2 January 2017 (e.g., Fig. 8c), with a stationary front extending east and a cold front extending to the southwest. SSTs along the Gulf coast are approximately 18-22°C, while temperatures near the center of the Gulf reach 26-28°C (e.g., Fig 8d). The 1200 UTC SPC Day 1 Convective Outlook (e.g., Fig. 8e) for this event includes an enhanced risk throughout most of Louisiana, Mississippi, southwest Alabama, and the far western Florida panhandle with a surrounding slight risk area that includes portions of eastern Texas, southeast Arkansas, western Georgia, and the rest of the Florida panhandle (NOAA 2017). SPC forecasters predict that all modes of severe weather are associated with an elevated risk across these areas. Radar analysis indicates the presence of disorganized convection ahead of the advancing cold front, as well as a well-formed bow echo along the cold front. These storms are centralized along the Gulf Coast, extending northward about midway through the Gulf Coast states. These storms result in 43 tornado reports, six hail reports, and 246 wind reports throughout eight states in the southeast United States (NOAA 2017; Fig. 8f).

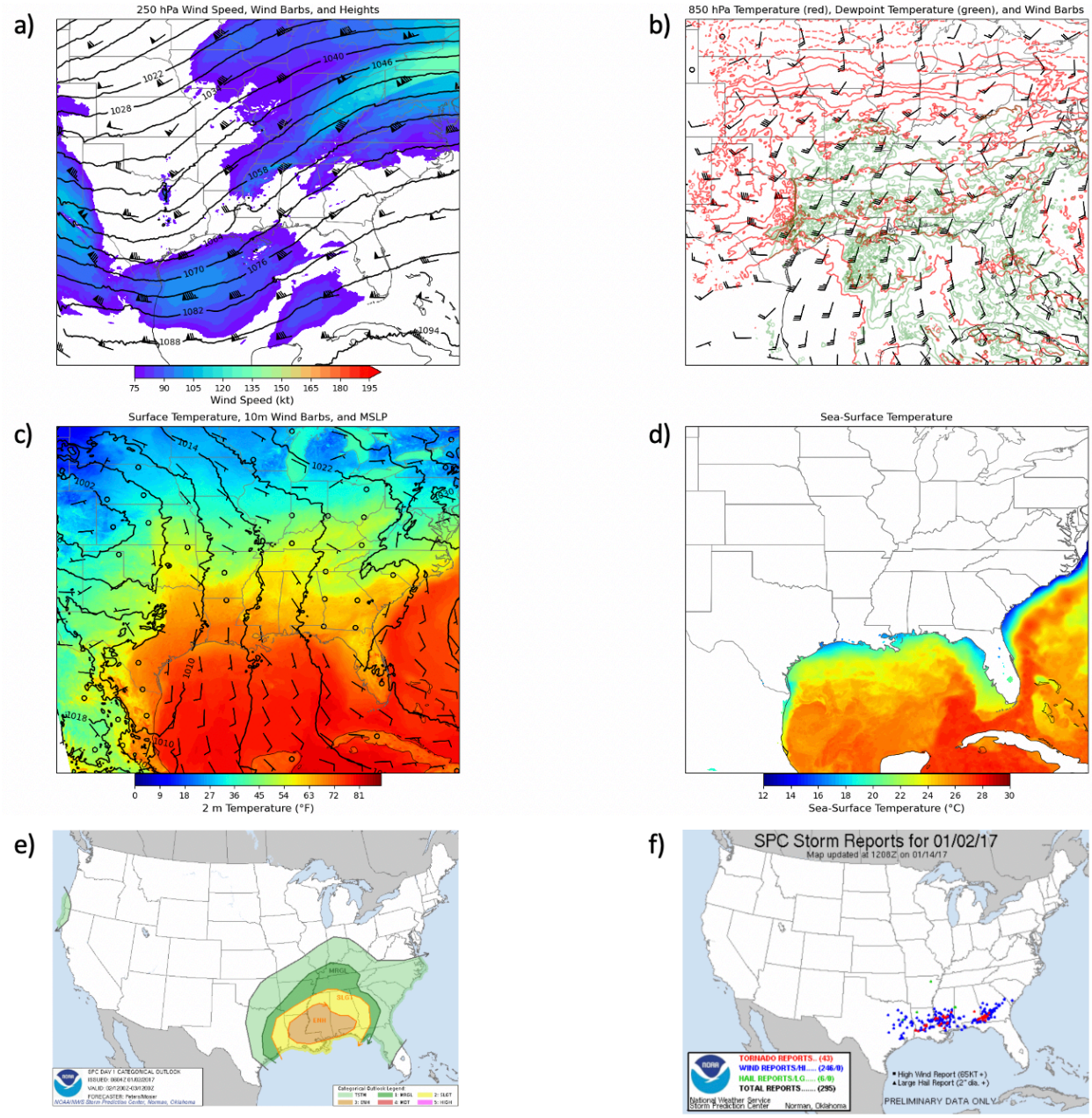

Figure 8: 1200 UTC 2 January 2017 analyses for: a) 250 hPa shaded wind speeds (kt), wind barbs (half-barb = 5 kt, full barb = 10 kt, pennant = 50 kt), and height contours (dm), b) 850 hPa temperature contours (red; °C), dewpoint temperature contours >8°C (green; °C), and height contours (dm), c) shaded surface temperature (°F), 10-m wind barbs (half-barb = 5 kt, full barb = 10 kt, pennant = 50 kt), and mean sea-level pressure contours (hPa), d) shaded SST (°C), e) SPC Day 1 Convective Outlook (contours) obtained by NOAA/NWS Storm Prediction Center, and f) Local Storm Reports (red=tornado, green=hail, blue=wind) obtained by NOAA/NWS Storm Prediction Center.

h. 21-22 January 2017

This two-day case is associated with two rounds of severe weather. The 250 hPa analysis (e.g., Fig. 9a) indicates a jet streak on the lee side of a broad trough with winds in excess of 125 kt located over east Texas and Arkansas at 0000 UTC 21 January 2017. This jet streak moves to the northeast through time as the exit region of a second northwest-to-southeast oriented jet streak situates itself over the southwest United States and the associated trough with these streaks deepens over the Midwest. 850 hPa analyses at 1200 UTC on 21 January 2017 (e.g., Fig. 9b) indicates the presence of a shortwave feature over Texas and Oklahoma. A lower-tropospheric low-pressure system develops between 0000 UTC 22 January and 0000 UTC 23 January 2017 and subsequently intensifies as it propagates eastward. Surface analysis at 0000 UTC 21 January 2017 indicates a weak area of low-pressure over Kansas, with a second, more intense area of low-pressure centered over the Dakotas. A weak stationary front is positioned across the Midwest, with a cold front to its northwest throughout the Dakotas and extending into Colorado. By 1200 UTC 21 January 2017 (e.g., Fig. 9c) a stationary front develops along the Gulf Coast and it is the evolution and progression of this front, coupled with the arrival of kinematic support from upper and mid-level jet streaks, that is responsible for the severe weather outbreak associated with this case. SSTs located in the Gulf of Mexico along the coast vary from approximately 17-21°C. Temperatures throughout much of the center of the Gulf are approximately 24°C, with some areas near the southeastern extent reaching almost 28°C (e.g., Fig 9d). The 1200 UTC 21 January 2017 SPC Day 1 Convective Outlook (e.g., Fig. 9e) has two separate areas under an enhanced risk for this case: (1) southeast Arkansas and northern Mississippi and (2) southern Alabama, southwest Georgia, and the Florida panhandle (NOAA 2017). A slight risk area encompasses both enhanced-risk areas, extending throughout the

remainder of Arkansas, portions of Louisiana, and east into Georgia and far southern South Carolina. Tornadoes, severe hail, and severe wind are considered risks in this event, with particular emphasis on the possibility for large hail due to steep lapse rates. The 1200 UTC 22 January 2017 SPC Day 1 Convective Outlook consists of a moderate risk located throughout southern Georgia, enhanced risk throughout much of Florida, southeastern Alabama, and most of South Carolina, and a slight risk surrounding these areas that also reach into North Carolina. The SPC refers to the coupling of a strong, 60+ kt, LLJ and the upper-level jet streak as the basis for increased severe weather potential. The radar analysis indicates convection, mostly in the form of individual cells, throughout east Texas and Louisiana early on 21 January 2017. The storms evolve into a QLCS-like system by 1100 UTC, with some preceding individual cells ahead of the advancing line. This line of storms intensifies as it propagates east through the Gulf Coast states. The evolution of the thunderstorms continues and a second QLCS forms throughout 22 January 2017. This second QLCS is responsible for the second round of severe weather that occurred with this event, in which the local storm reports are located primarily throughout Alabama, Georgia, and Florida. This event is responsible for a total of 85 tornado reports, 75 hail reports, and 233 wind reports (NOAA 2017; Fig. 9f).

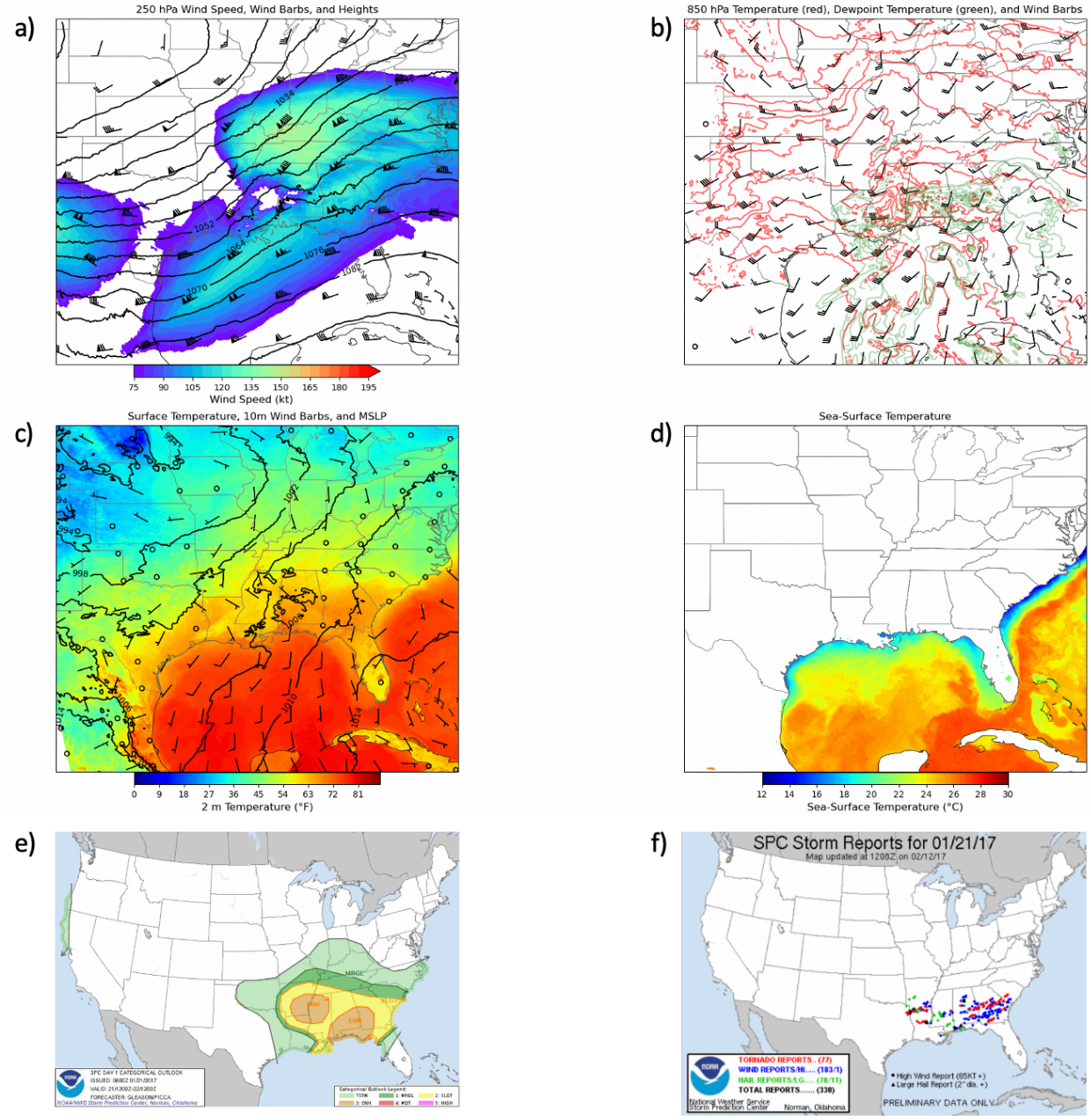

Figure 9: 1200 UTC 21 January 2017 analyses for: a) 250 hPa shaded wind speeds (kt), wind barbs (half-barb = 5 kt, full barb = 10 kt, pennant = 50 kt), and height contours (dm), b) 850 hPa temperature contours (red; °C), dewpoint temperature contours >8°C (green; °C), and height contours (dm), c) shaded surface temperature (°F), 10-m wind barbs (half-barb = 5 kt, full barb = 10 kt, pennant = 50 kt), and mean sea-level pressure contours (hPa), d) shaded SST (°C), e) SPC Day 1 Convective Outlook (contours) obtained by NOAA/NWS Storm Prediction Center, and f) Local Storm Reports (red=tornado, green=hail, blue=wind) obtained by NOAA/NWS Storm Prediction Center.

4. Results

While the correct placement and evolution of the surface fronts, precipitation, and storm features is important in establishing an acceptable control simulation for further analysis of each severe-weather event, this study's goal of quantifying forecast sensitivities does not require that the control simulations perfectly match reality. The steps taken that are detailed below ensure the control simulations are *representative* of the observed weather evolution and is done to ensure a measure of confidence that the obtained forecast sensitivities are realistic.

A visual comparison between the control simulation, observed conditions, and analyses for each case is completed to ensure an acceptable control simulation has been established before conducting the full ensemble of simulations. To conduct this comparison, plots of surface variables (mean sea-level pressure (MSLP), temperature, dewpoint temperature, and wind barbs), radar reflectivity, and UH were created. These plots were then compared with observational and analysis data from the SPC's archive database to ensure that the control simulations represented the correct approximate placement and evolution of the different weather features for each case. In the cases that depart from a 0000 UTC initialization time, it was determined that adjusting the initialization time was necessary to better simulate a more accurate progression of the event's weather.

Once the control simulations were subjectively deemed acceptable and the eight cases' worth of ensemble simulations were completed, analysis was necessary to determine which simulation exhibited the most variability between the cases so that the second method (described in Section 3c above) used in this study could be completed. The 13 October 2014 case was associated with the greatest ensemble variability amongst the eight cases. This variability is most prominent when comparing UH (the other surface variables used in the comparison process also

indicated differences among the ensemble members but are not shown here). Figure 10 below shows an example of the differences associated with UH placement and intensity for four different cases: 13 October 2013 (a), 21 January 2017 (b), 10 February 2013 (c), and 4 April 2011 (d). The simulated UH for the 21 January 2017 and 10 February 2013 cases display the UH almost directly on top of one another. While the intensities of the UH may vary, the locations do not vary much in comparison to the 13 October 2014. The vast area of differences in the production of UH exhibited in this case were ultimately what led to the decision to choose this case for further analysis. There are several areas in which one SST produced UH that was unique to that specific SST simulation, as opposed to all simulations producing UH in the same area. Additionally, the RM-DTE analysis below also supports this decision based on the ensemble spread compared with the other eight cases.

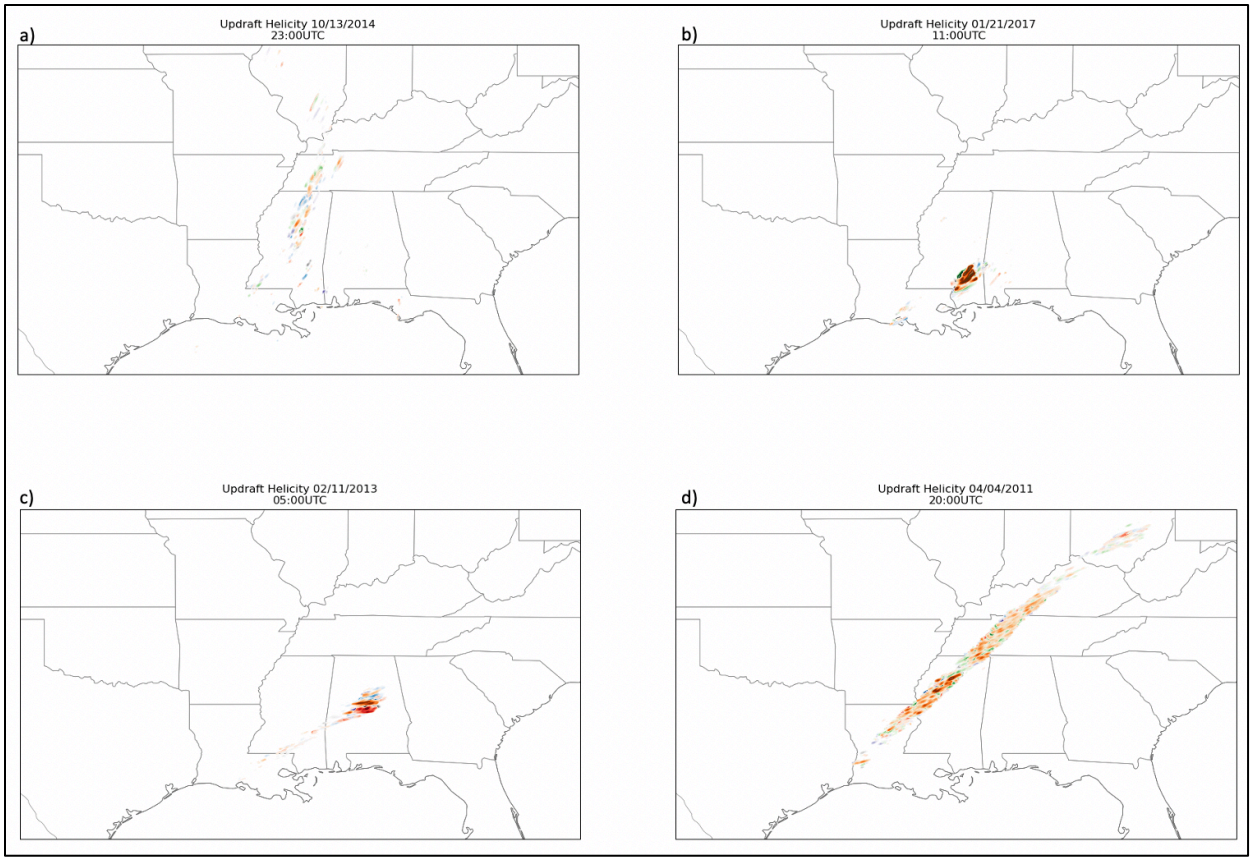

Figure 10: Shaded hourly maximum UH ($m^{-2}s^{-2}$) for cases: a)13 October 2014, b) 21 January 2017, c) 10 February 2013, and d) 4 April 2011. Each color depicts a different SST simulation with panels b-d depicting evidence of the minimal variability of UH placement among the six ensemble members.

a. RM-DTE

i. SST Sensitivity Ensembles

In general, the highest-magnitude spread (> 10 m s^{-1}) is centralized along the advancing lines of simulated thunderstorms in each case, with lower-magnitude (~1-3m s^{-1}) differences behind the line in the trailing stratiform regions and along associated warm fronts, although these differences are likely due to numerically induced chaos rather than having a physical driver. This finding is seen in all the RM-DTE plots, across the 108 simulations, and is consistent with the findings from past studies (Sippel and Zhang 2008). In cases where the severe weather threat originates away from the Gulf of Mexico, such as on 4 April 2011 (Fig. 11a), there are little to no

additional areas of ensemble spread exceeding 1 m s^{-1}. However, in cases where the severe weather threat originates close to the northern Gulf of Mexico coast, such as on 13 October 2014, the RM-DTE plots indicate additional ensemble spread that is located ahead of the main lines of convection. These cases' ensemble spreads are more widespread and disorganized than those whose severe threats originate away from the Gulf of Mexico. This suggests the SST may be, in part, influencing the forecasts. The thermodynamic environment is likely changing with the southerly flow over the Gulf of Mexico carrying moisture rich air parcels into the Gulf Coast states. The 25 December 2012 case is a prime example of increased ensemble spread emanating from the Gulf of Mexico ahead of an advancing QLCS (Fig. 11b). Figure 11b below depicts forecast hour 15, where there is an area of differences of low magnitudes ahead of the main line, as well as widespread differences throughout Louisiana, Mississippi, Alabama, and Georgia that propagated northward in the preceding forecast times (not shown).

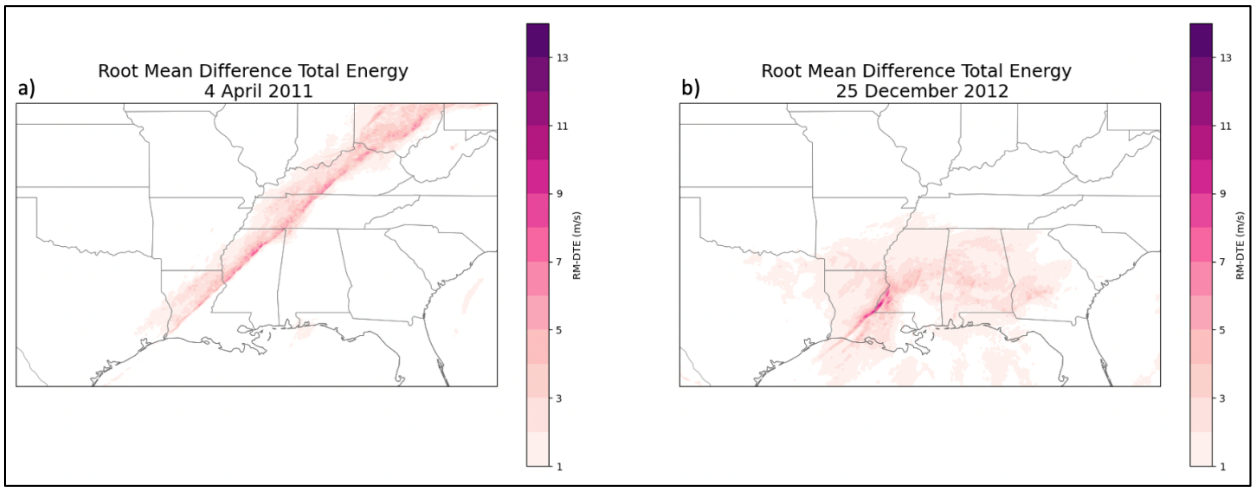

Figure 11: Shaded RM-DTE (ms^{-1}) at (a) forecast hour 20 on 4 April 2011 and (b) forecast hour 15 on 25 December 2012.

Another common characteristic between cases occurs where multiple lines of storms move through an area or widespread convection is occurring. In these cases, the RM-DTE is often widespread and disorganized, particularly after the initial convection propagates through an

area. A representative example is given by the ensemble-spread progression in the 21-22 January 2017 case (Fig. 12), in which an initial line of storms move throughout the Gulf Coast states before a second round of storms propagates through the same area. The ensemble spread becomes more widespread but smaller in magnitude throughout the simulation. It is hypothesized that the effects of the initial storms on their environments contribute to the subsequent increased spread in these cases. Due to the nature of these cases, it is hard to discern how much the SST may be affecting the forecasts without further analysis.

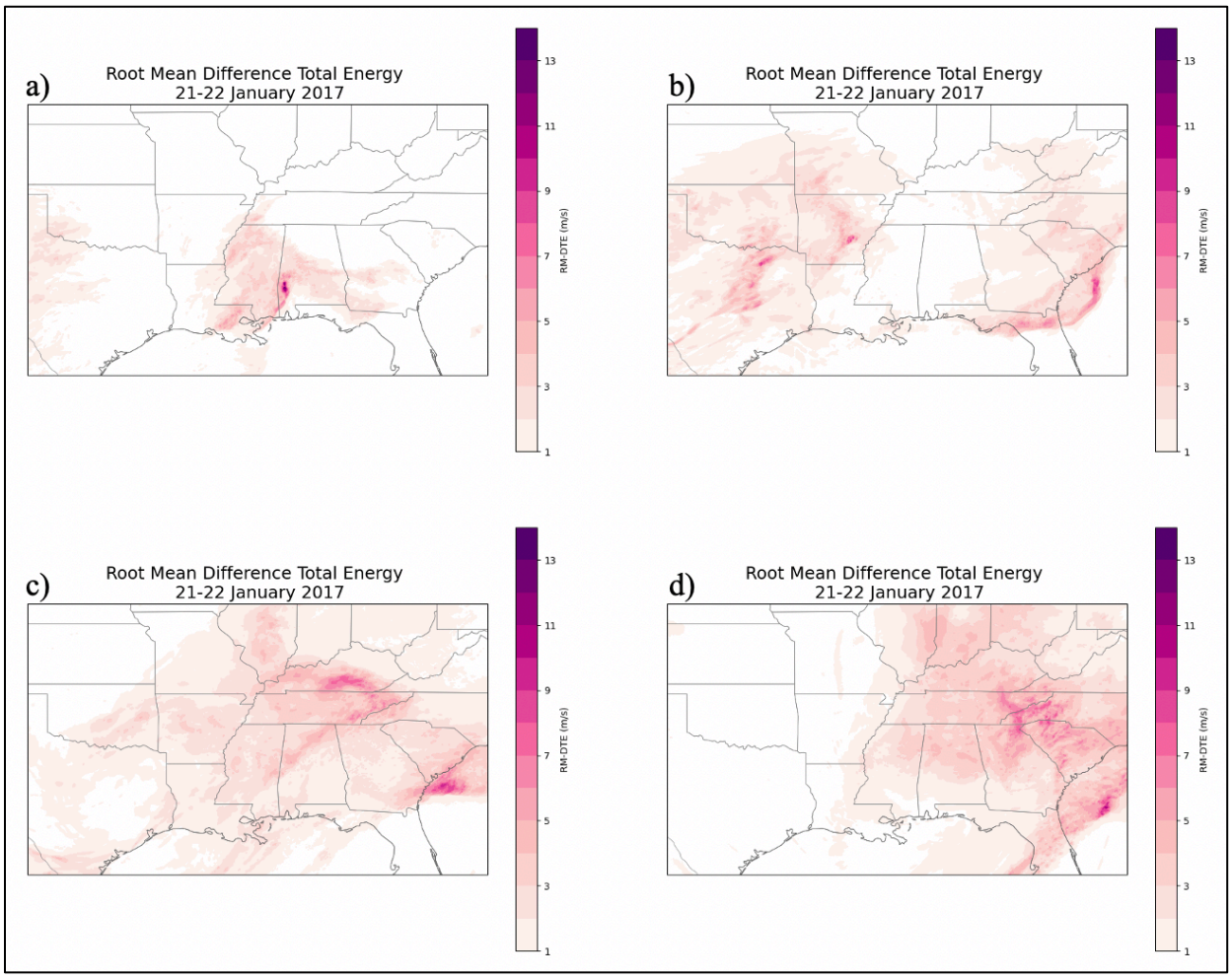

Figure 12: Shaded RM-DTE (ms^{-1}) for 21-22 January 2017 at forecast hours: a) 12, b) 24, c) 36, and d) 42.

ii. SST vs. Atmospheric Sensitivity Ensembles

To analyze the SST versus atmospheric sensitivity simulations, RM-DTE calculations and plots are generated in two ways; holding the atmospheric conditions constant and allowing the SST to be variable (i.e., ensemble consists of six members; one ERA5 ensemble member simulation (control) and the five SST simulations initialized with the same ERA5 ensemble member for the atmospheric conditions) and holding the SST constant and allowing for variable atmospheric conditions (i.e., ensemble consists of ten members; simulations initialized with the same SST dataset and each of the ten ERA5 ensemble members for the atmospheric conditions).

Holding the atmospheric conditions constant and allowing for variability in SSTs results in ensemble spread that is closely related to that seen in the SST sensitivity plots above. This is to be expected since the SST sensitivity plots also included only one dataset to represent the atmospheric conditions. One discernable difference is that each of the ten members ensembles exhibit generally narrower areas of high magnitude RM-DTE values. There is also a tendency for the differences to be greater in magnitude along the QLCS, some forecast hours depicting values > 4 ms^{-1}, in the atmospheric sensitivity case. An example of these differences at forecast hour 12 is shown in Fig. 13 below. Note how the area experiencing the greatest ensemble spread is confined to a thin line in each of the different members shown (panels b-e). Comparing panels b-e also highlights some of the differences exhibited between different atmospheric members. Each individual member's ensemble evolves the QLCS slightly differently, with some members exhibiting a strong bowing feature to the line, and the locations of the greatest ensemble spread differing in location between the members, indicating differences between the members on the placement of the strongest areas of convection. These findings provide helpful insight to the

effects of the atmospheric variability between different members when all SSTs are considered in the ensemble.

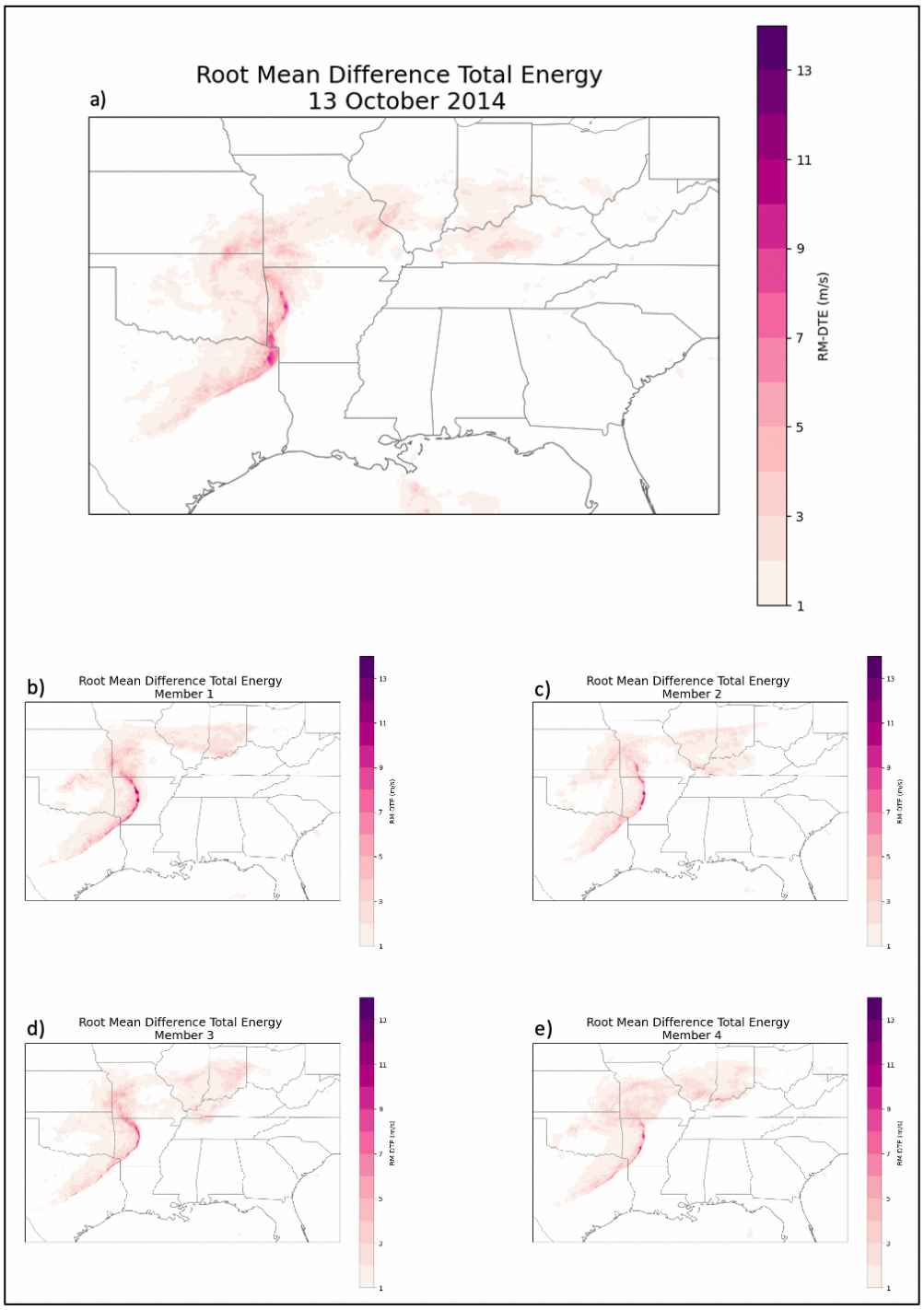

Figure 13: Shaded RM-DTE (ms^{-1}) on 13 October 2014 for forecast hour 12 for: a) the SST sensitivity simulations and the 10-member constant atmospheric conditions ensembles (variable SSTs) using members: b), 1, c) 2, d) 3, and e) 4.

When holding the SST constant, the resulting ensemble spread is spatially more expansive than what is seen in the two previous subsections (e.g., Fig. 14). Additionally, the magnitudes of the differences are greater at early hours in the simulation period, especially along the advancing QLCS. Although the overall characteristics of the ensemble spread are consistent between the two ensembles, the variable atmospheric conditions allow for increased spread extent and magnitude as compared to the variable SST initializations. The only other differences between the ensembles occurs between forecast hours 16-19, where small differences happen along the Louisiana coast. Despite these differences being minimal, they do suggest that the forecasts may be sensitive to the SSTs, since each simulation includes the same ten member's atmospheric conditions, but yet the fixed SSTs themselves exhibit changes between them.

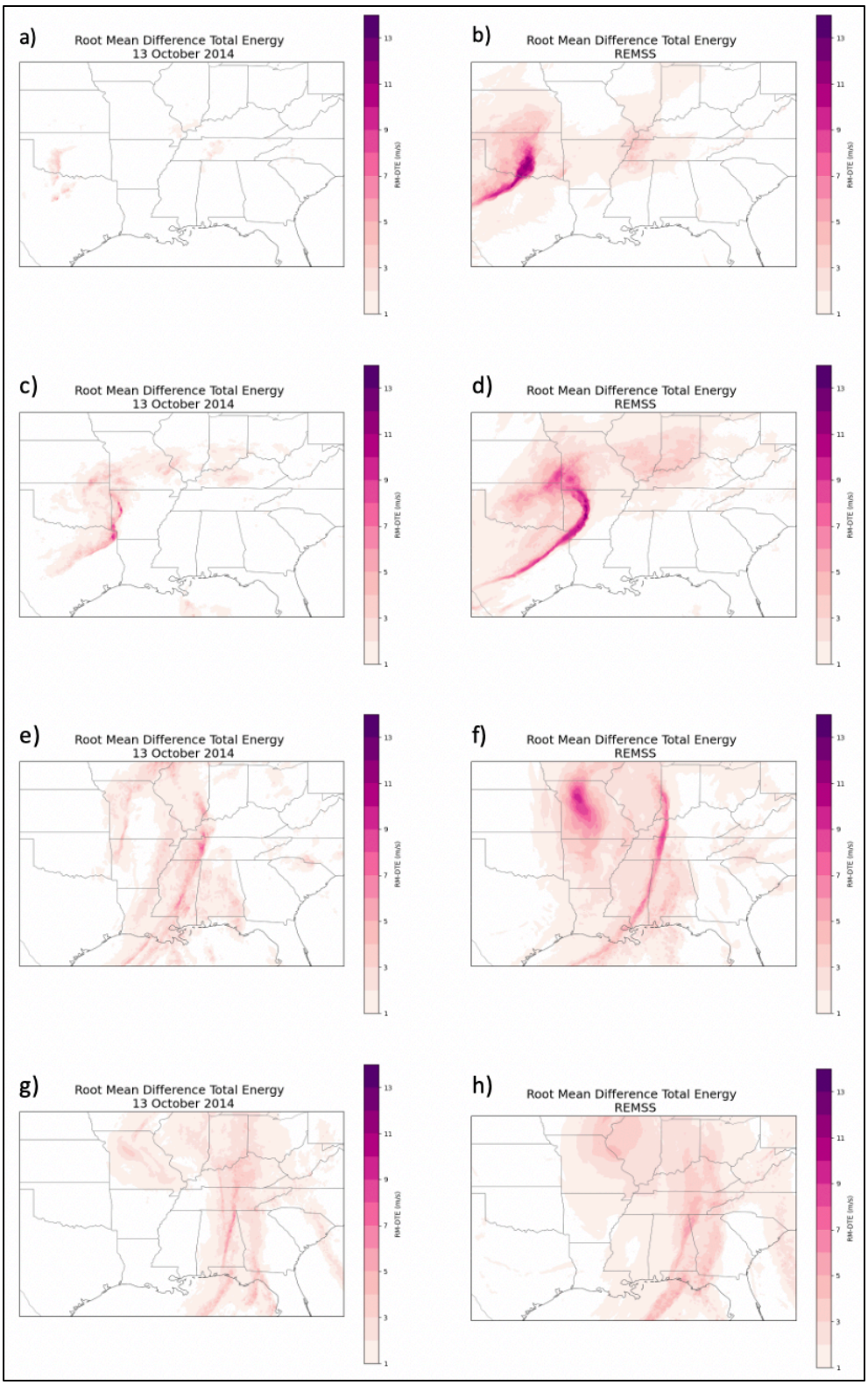

Figure 14: Shaded RM-DTE (ms^{-1}) on 13 October 2014 for the SST sensitivity simulations (left panels) and SST vs. atmospheric simulations holding REMSS constant (right panels) for forecast hours; a,b) 06, c,d) 12, e,f) 24, and g,h) 36.

b. FSS

When comparing the SST sensitivity ensembles and the atmospheric versus SST sensitivity ensemble results below, we focus primarily on the 99th percentile threshold of 33.4 m^{-2} s^{-2}. Some general characteristics were apparent when comparing the FSSs between all 108 simulations (384 calculations total). The discussion of the results in the subsections below will focus on the 9-point neighborhoods (with ~120 km radii), since these results are likely more representative of the skill that can be gained from this analysis and used for improvements to operational CAMs. A common characteristic is in the skill between the SSTs. No one SST dataset was more skillful than another, which suggests that the verification is likely capturing meaningful skill variability across the simulations for each case.

There are also some important points to keep in mind when interpreting the resulting FSSs in this study. This study computed the FSS on an 80 km x 80 km grid, which involved extrapolating the point observations and the UH swaths to a coarse binary grid. While the 80 km x 80 km grid is equivalent to the SPC's probabilistic outlook grid, the process used in this study will inherently wash out the smaller scale differences that may be apparent if a finer grid scale is used, which likely will affect the resulting skill. Additionally, measures were not taken to eliminate UH that was produced over the ocean, so decreased skill scores are to be expected in the cases where UH occurs over the water since LSRs cannot occur there. For the purposes of this discussion and with the above points in mind, scores < 0.5 are considered "low skill" (Roberts and Lean 2008).

i. SST Sensitivity Ensembles

The SST sensitivity simulations experienced the lowest skill at the 10.1 $m^{-2}s^{-2}$ threshold for all cases except 4 April 2011, in which the lowest skill is at 78.6 $m^{-2}s^{-2}$. Low skill at the 95th

percentile threshold in all ensembles is due to an over-production of UH compared to the LSRs, with the opposite problem of too little UH to LSR ratio leading to additional low skill values in the 4 April 2011 case (Fig. 15). While UH is commonly used as a severe weather proxy for tornadoes and hail, it is not a reliable indicator of severe wind capabilities within a storm. Wind damage can result from non- or weakly rotating phenomena, such as QLCSs or mesoscale convective systems, and the use of UH as a prognosis for mid-level rotation does not directly relate to indications of severe wind capabilities (Kain et al. 2008). This case was associated with over 300 severe wind reports and the LSRs associated with this case cover almost the entire southeastern United States as a result. For this reason, the skill scores are likely marred by the inclusion of the wind reports more so than the other seven cases in which the wind reports are not as extensive and therefore likely do not negatively affect the resulting skill score as severely as on 4 April 2011.

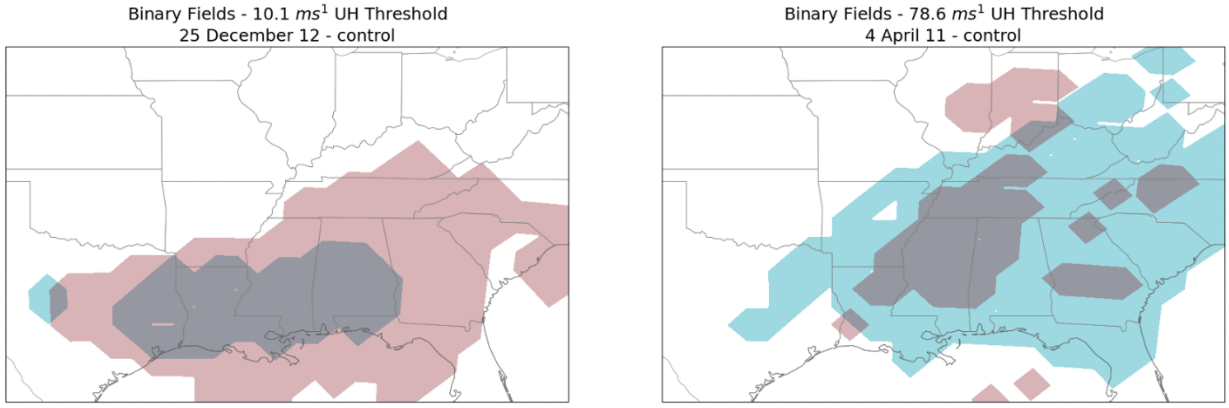

Figure 15: SST simulation binary (yes/no) fields of gridded LSRs (blue) and gridded control simulation UH (red) for (left) 25 December 2012 and (right) 4 April 2011.

The skill scores for 7 March 2008 and 16-17 November 2014 were considerably lower than all other cases, with an average skill value at the 33.4 $m^{-2}s^{-2}$ threshold equaling 0.234 and 0.235 respectively. In these cases, the low skill is due, in part, to a displacement of the simulated

UH in which the UH is too far south and on 7 March 2008 extends too far east. The displacement of the UH is only apparent in these two cases, the other six cases' UH is centralized over the same area where LSRs occur. Out of the eight cases, the highest skill was 0.795 on 4 April 2011, but this finding is likely untrustworthy due to the inclusion of the vast number of severe wind reports in the analysis process. The next highest skill score occurs on 13 October 2014 with a value of 0.748. Three additional cases have average skill scores > 0.5, which indicate that the ensemble of forecasts is skillful, regardless of the negative effects of UH over the ocean and inclusion of wind reports. The overall skill spread between ensemble members at the 99th percentile is relatively low, with the average spread for all cases equal to 0.083. This finding shows that the SST members do not differ greatly from one another in terms of their skill. The 99th percentile skill scores for these ensembles is depicted in Table 4 below. With the coarse grid used for these analyses, it is likely that this result would change significantly on a finer grid.

FSS Metrics - SST Sensitivity		
	Spread	**Average**
7-Mar-08		
33.4	0.024	0.234
4-Apr-11		
33.4	0.047	0.795
25-Dec-12		
33.4	0.177	0.665
10-Feb-13		
33.4	0.049	0.454
13-Oct-14		
33.4	0.051	0.748
16-Nov-14		
33.4	0.095	0.235
2-Jan-17		
33.4	0.048	0.650
21-Jan-17		
33.4	0.176	0.519

Table 4: FSS ensemble spread and ensemble averages for SST sensitivity simulations.

ii. SST vs. Atmospheric Sensitivity Ensembles

When comparing the atmospheric sensitivity (ERA5-based) simulations FSSs (variability across SST ensembles vs. variability across atmospheric ensembles) the 99th percentile threshold revealed a total average skill score of 0.776. The SST variability ensembles (Table 5) had a skill spread between 0.006 and 0.064, with an average skill score spread of only 0.035 while the atmospheric variability ensembles (Table 6) had a skill spread between 0.037 and 0.083, with an average skill score spread of 0.060. These findings indicate a 0.021 increase in ensemble spread in the atmospheric variable ensembles. This finding is consistent with our hypothesis that the skill score variation would be greater across the atmospheric variable simulations than the SST variable simulations, due to the introduction of atmospheric uncertainty that is absent from the SST variable simulations. Since this study is conducted on a coarse grid, we also expected the differences found between ensembles would be small.

FSS Metrics - Atmospheric Sensitivity Simulations - Variable SST					
	Spread - 9	**Average - 9**		**Spread - 9**	**Average - 9**
MEM 1			**MEM 6**		
33.4	0.054	0.774	**33.4**	0.026	0.771
MEM 2			**MEM 7**		
33.4	0.018	0.786	**33.4**	0.035	0.767
MEM 3			**MEM 8**		
33.4	0.064	0.791	**33.4**	0.017	0.791
MEM 4			**MEM 9**		
33.4	0.053	0.790	**33.4**	0.055	0.748
MEM 5			**MEM 10**		
33.4	0.060	0.772	**33.4**	0.006	0.772

Table 5: FSS ensemble spread and ensemble averages for atmospheric sensitivity simulations with variable SSTs.

FSS Metrics - Atmospheric Sensitivity Simulations - Variable Atmospheric Conditions		
	Spread - 9	**Average - 9**
CONTROL		
33.4	0.083	0.778
GHRSST		
33.4	0.053	0.771
NOAAOI		
33.4	0.037	0.772
USNO		
33.4	0.066	0.784
REMSS		
33.4	0.074	0.772
FNMOC		
33.4	0.045	0.781

Table 6: FSS ensemble spread and ensemble averages for atmospheric sensitivity simulations with variable atmospheric conditions.

5. Conclusions

This study consisted of a two-method approach to quantify SST sensitivity and the effects of ocean-state uncertainty on severe weather forecasts in HSLC environments in the southeast United States. Severe weather outbreaks in HSLC environments are rare in comparison to outbreaks associated with greater instability, rendering research into characteristics driving HSLC severe weather and modeling challenges in these environments necessary.

Eight cases in which severe weather threats posed significant forecast and warning challenges to WFO's in Louisiana, Alabama, and Florida, were considered in this study. Six-member ensemble forecasts with varying SST datasets were produced using the WRF-ARW and analyzed to provide an estimate of the overall SST uncertainty effects. Additionally, the case that produced the most variability in a variety of subjective analyses, 13 October 2014, was used to further investigate and quantify the ocean-state uncertainties on CAM forecasts. This portion of

the project consisted of a 60-member ensemble of forecasts that accounted for SST uncertainty as well as atmospheric state uncertainty.

Analysis of the two different ensembles revealed that cases in which the severe weather threat originates near the Gulf Coast resulted in slightly larger ensemble spread ahead of advancing lines of convection. This suggests that SSTs may be influencing the forecasts along and directly inland from the Gulf of Mexico, although more analysis is needed to determine the significance these possible influences have on the forecasts. The inclusion of atmospheric variability in the ensemble displayed a substantial increase in ensemble spread. The FSS revealed that the overall skill spread between ensemble members of the SST sensitivity simulations from method one was 0.083, indicating little skill difference between individual SST members. When comparing the atmospheric sensitivity simulations, our findings were consistent with our hypothesis, for which these simulations experienced increased ensemble spread (0.039 vs. 0.060) with the inclusion atmospheric variability. Additionally, the FSS analysis revealed that at the lowest UH threshold, too much UH is produced and leading to low skill scores. There were also two cases in which the UH was displaced from the LSRs, which consequently led to low skill scores.

In conclusion, there is some evidence to suggest that SST uncertainty may affect forecasts of severe weather in the southeast United States, particularly near the Gulf Coast. However, due to the limits associated with the processes used in this study, a definitive quantification of the influences of these uncertainties cannot be determined. Future work will continue to refine the preliminary results discussed thus far. Some of this work includes processing the LSRs and UH on a finer scaled grid to capture the small-scale variations that are likely being smoothed away by using a larger grid. Recalculating the RM-DTE and FSS on the

finer grid to see if more insight can be attained as to how much ocean-state uncertainties could be affecting severe weather forecasts. Thermodynamic characteristics of near-shore variables can also be analyzed to support any findings.

References

Ashley, W. S., A. J. Krmenec, and R. Schwantes, 2008: Vulnerability due to nocturnal tornadoes. *Wea. Forecasting*, **23**, 795–807, https://doi.org/10.1175/2008WAF2222132.1.

Adams-Selin, R. D., S. C. van den Heever, and R. H. Johnson, 2013: Sensitivity of Bow-Echo Simulation to Microphysical Parameterizations, *Wea. Forecasting*, **28,** 1188-1209, doi: 10.1175/WAF-D-12-00108.1

Anderson-Frey, A., Y. Richardson, A. Dean, R. Thompson, and B. Smith, 2016: Investigation of near-storm environments for tornado events and warnings. *Wea. Forecasting*, **31**, 1771–1790, https://doi.org/10.1175/WAF-D-16-0046.1.

Anderson-Frey, A., Y. Richardson, A. Dean, R. Thompson, and B. Smith, 2018: Near-storm environments of outbreak and isolated tornadoes. *Wea. Forecasting*, **33**, 1397–1412, https://doi.org/10.1175/WAF-D-18-0057.1.

Anderson-Frey, A., and H. Brooks, 2019: Tornado fatalities: An environmental perspective. *Wea. Forecasting*, **34**, 1999–2015, https://doi.org/10.1175/WAF-D-19-0119.1.

Anderson-Frey, A., Y. Richardson, A. Dean, R. Thompson, and B. Smith, 2019: Characteristics of tornado events and warnings in the southeastern United States. *Wea*. *Forecasting*, **34**, 1017–1034, https://doi.org/10.1175/WAF-D-18-0211.1.

Benjamin, S. G., and Coauthors, 2016: A North American Hourly Assimilation and Model Forecast Cycle: The Rapid Refresh, *Mon. Wea. Rev.*, **144,** 1669-1694, https://doi.org/10.1175/MWR-D-15-0242.1.

Berner, J., K. R. Smith, S.-Y. Ha, J. Hacker, and C. Snyder, 2015: Increasing the skill of probabilistic forecasts: Understanding performance improvements from model-error representations. *Mon. Wea. Rev.*, **143**, 1295–1320, doi:10.1175/MWR-D-14-00091.1.

Burlingame, B. M., C. Evans, and P. J. Roebber, 2017: The influence of PBL parameterization on the practical predictability of convection initiation during the Mesoscale Predictability Experiment (MPEX). *Wea. Forecasting*, **32**, 1161–1183, https://doi.org/10.1175/WAF-D-16-0174.1.

Chen, F., and J. Dudhia, 2001: Coupling an Advanced Land Surface–Hydrology Model with the Penn State–NCAR MM5 Modeling System. Part I: Model Implementation and Sensitivity, *Mon. Wea. Rev.*, **129,** 569-585, doi: https://doi.org/10.1175/1520-0493(2001)129<0569:CAALSH>2.0.CO;2

Chin, T. M., J. Vazquez-Cuervo, and E. M. Armstrong, 2017: A multi-scale high-resolution analysis of global sea surface temperature. *Remote Sens. Environ.*, **200**, 154–169, https://doi.org/10.1016/j.rse.2017.07.029.

Clark, A. J., and Coauthors, 2018: The Community Leveraged Unified Ensemble (CLUE) in the 2016 NOAA/Hazardous Weather Testbed Spring Forecasting Experiment. *Bull. Amer. Meteor. Soc.*, **99,** 1433–1448, https://doi.org/10.1175/BAMS-D-16-0309.1.

Cohen, A. E., S. M. Cavallo, M. C. Coniglio, and H. E. Brooks, 2015: A review of planetary boundary layer parameterization schemes and their sensitivity in simulating southeastern U.S. cold season severe weather environments. *Wea. Forecasting*, **30**, 591–612, doi:10.1175/WAF-D-14-00105.1.

Cope, A. M., 2004: An early morning mid-Atlantic severe weather episode: Short-lived tornadoes in a high-shear low-instability environment. Preprints, *22nd Conf. on Severe Local Storms,* Hyannis, MA, Amer. Meteor. Soc., P1.4. [Available online at https://ams.confex.com/ams/11aram22sls/webprogram/Paper81834.html.]

Cummings, J. A., and O. M. Smedstad, 2013: Variational data assimilation for the global ocean. *Data Assimilation for Atmospheric, Oceanic and Hydrologic Applications*, S. K. Park and L. Xu, Eds., Vol. II, Springer, 303–343.

Davies, J. M., 1993: Hourly helicity, instability, and EHI in forecasting supercell tornadoes. Preprints, *17th Conf. on Severe Local Storms,* St. Louis, MO, Amer. Meteor. Soc., 107–111.

Donlon, C., and Coauthors, 2007: The Global Ocean Data Assimilation Experiment High-resolution Sea Surface Temperature Pilot. *Bull. Amer. Meteor. Soc.*, **88,** 1197–1213.

Evans, J. S., and C. A. Doswell III, 2001: Examination of derecho environments using proximity sounding. *Wea. Forecasting*, **16,** 329–342.

Grunzke, C. T., and C. Evans, 2017: Predictability and dynamics of warm-core mesoscale vortex formation with the 8 May 2009 "Super Derecho" event. *Mon. Wea. Rev.*, **145**, 811–832, https://doi.org/10.1175/MWR-D-16-0217.1.

Guyer, J. L., and A. R. Dean, 2010: Tornadoes within weak CAPE environments across the continental United States. *25th Conf. on Severe Local Storms*, Denver, CO, Amer. Meteor. Soc., 1.5, https://ams.confex.com/ams/25SLS/techprogram/paper_175725.htm.

Ha, S., J. Berner, and C. Snyder, 2015: A comparison of model error representations in mesoscale ensemble data assimilation. *Mon. Wea. Rev.*, **143**, 3893–3911, https://doi.org/10.1175/MWR-D-14-00395.1.

Hersbach, H., and Coauthors, 2018: ERA5 hourly data on pressure levels from 1979 to present. Copernicus Climate Change Service (C3S) Climate Data Store (CDS). 10.24381/cds.bd0915c6.

Huang, B., Liu, C., Freeman, E., Graham, G., Smith, T., and H. Zhang, 2021: Assessment and Intercomparison of NOAA Daily Optimum Interpolation Sea Surface Temperature (DOISST) Version 2.1, *J. of Climate*, **34,** 7421-7441, https://doi.org/10.1175/JCLI-D-21-0001.1.

Iacono, M. J., J. S. Delamere, E. J. Mlawer, M. W. Shepard, S. A. Clough, and W. D. Collins, 2008: Radiative forcing by long-lived greenhouse gases: Calculations with the AER radiative transfer models. *J. Geophys. Res.*, 113 .D13103, doi:10.1029/2008JD009944.

Janjic, Z. I., and R. Gall, 2012: Scientific documentation of the NCEP Nonhydrostatic Multiscale Model on the B Grid (NMMB). Part 1: Dynamics. NCAR/TN-489+STR, 75 pp. [Available online at http://nldr.library.ucar.edu/repository/assets/technotes/TECH-NOTE-000-000-000-857.pdf.]

King, J. R., M. D. Parker, K. D. Sherburn, and G. M. Lackmann, 2017: Rapid evolution of cool season, low-CAPE severe thunderstorm environments. *Wea. Forecasting*, **32**, 763–778, https://doi.org/10.1175/WAF-D-16-0141.1.

Lane, J. D., and P. D. Moore, 2006: Observations of a non-supercell tornadic thunderstorm from terminal Doppler weather radar. Preprints, *23rd Conf. on Severe Local Storms,* St. Louis, MO, Amer. Meteor. Soc., P4.5. [Available online at https://ams.confex.com/ams/pdfpapers/115102.pdf.]

Lawson, J., and W. A. Gallus Jr., 2016: On Contrasting Ensemble Simulations of Two Great Plains Bow Echoes, *Wea. Forecasting*, **31,** 787-810, doi: 10.1175/WAF-D-15-0060.1

Martin, M., and Coauthors, 2012: Group for High Resolution Sea Surface Temperature (GHRSST) analysis fields inter-comparisons. Part 1: A GHRSST multi-product ensemble (GMPE). *Deep-Sea Res. II*, **77**, 21–30, doi:10.1016/j.dsr2.2012.04.013.

McAvoy, B. P., W. A. Jones, and P. D. Moore, 2000: Investigation of an unusual storm structure associated with weak to occasionally strong tornadoes over the eastern United States. Preprints, *20th Conf. on Severe Local Storms,* Orlando, FL, Amer. Meteor. Soc., 182–185.

Melhauser, C., and F. Zhang, 2012: Practical and intrinsic predictability of severe and convective weather at the mesoscales. *J. Atmos. Sci.*, **69**, 3350–3371, doi:10.1175/JAS-D-11-0315.1.

Metzger, E. J., and Coauthors, 2014: US Navy operational global ocean and arctic ice prediction systems. Oceanography, **27,** 32–43, https://doi.org/10.5670 /oceanog.2014.66.

Molina, M. J., J. T. Allen, and V. A. Gensini, 2018: The Gulf of Mexico and ENSO influence on subseasonal and seasonal CONUS winter tornado variability. *J. Appl. Meteor. Climatol.*, 57, 2439–2463, https://doi.org/10.1175/JAMC-D-18-0046.1.

Molina, M. J., & J. T. Allen, 2019: On the Moisture Origins of Tornadic Thunderstorms, *J. of Climate*, **32,** 4321-4346, https://doi.org/10.1002/2016GL071603.

Molina, M. J., J. T. Allen, and A. F. Prein, 2020: Moisture Attribution and Sensitivity Analysis of a Winter Tornado Outbreak, *Wea. Forecasting*, **35,** 1263-1288, doi: https://doi.org/10.1175/WAF-D-19-0240.1.

Nakanishi, M., and H. Niino, 2006: An improved Mellor–Yamada level-3 model: Its numerical stability and application to a regional prediction of advection fog. *Bound.-Layer Meteor.*, **119,** 397–407.

NOAA, 2021: SPC Convective Outlooks. Accessed 14 November 2021. https://www.spc.noaa.gov/products/outlook/archive/.

NOAA, 2021: SPC Storm Reports. Accessed 14 November 2021. https://www.spc.noaa.gov/climo/reports/.

Paul, B. K., V. T. Brock, S. Csiki, and L. Emerson, cited 2003: Public response to tornado warnings: A comparative study of the May 4, 2003, Tornadoes in Kansas, Missouri, and Tennessee. Natural Hazards Research and Applications Information Center Quick Response Rep. 165. [Available online at http://www.colorado.edu/hazards/research/qr/qr165/qr165.html].

Parker, M. D., 2012: Impacts of lapse rates on low-level rotation in idealized storms. *J. Atmos. Sci.*, **69**, 538–559, doi:10.1175/JAS-D-11-058.1.

Powers, J. G., and Coauthors, 2017: The Weather Research and Forecasting Model: Overview, system efforts, and future directions. *Bull. Amer. Meteor. Soc.*, **98,** 1717– 1737, https://doi.org/10.1175/BAMS-D-15-00308.1.

Rasmussen, E. N., and D. O. Blanchard, 1998: A baseline climatology of sounding-derived supercell and tornado forecast parameters. *Wea. Forecasting*, **13**, 1148–1164, doi:10.1175/1520-0434(1998)013<1148:ABCOSD>2.0.CO;2.

REMSS, 2021: Microwave OI SST Product Description, Accessed 1 February 2020, remss.com

Reynolds, R. W., T. M. Smith, C. Liu, D. B. Chelton, K. S. Casey, and M. G. Schlax, 2007: Daily high-resolution blended analyses for sea surface temperature. *J. Climate*, **20,** 5473–5496.

Reynolds, R. W., and D. B. Chelton, 2010: Comparisons of daily sea surface temperature analyses for 2007–08. *J. Climate*, **23**, 3545–3562, doi:10.1175/2010JCLI3294.1.

Reynolds, C. A., R. Langland, P. M. Pauley, and C. Velden, 2013: Tropical cyclone data impact studies: Influence of model bias and synthetic observations. *Mon. Wea. Rev.*, **141,** 4373–4394, https://doi.org/10.1175/MWR-D-12-00300.1.

Romine, G. S., C. S. Schwartz, C. Snyder, J. L. Anderson, and M. L. Weisman, 2013: Model bias in a continuously cycled assimilation system and its influence on convection-permitting forecasts. *Mon. Wea. Rev.*, **141**, 1263–1284, doi:10.1175/MWR-D-12-00112.1.

Romine, G. S., C. S. Schwartz, J. Berner, K. R. Fossell, C. Snyder, J. L. Anderson, and M. L. Weisman, 2014: Representing Forecast Error in a Convection-Permitting Ensemble System, *Mon. Wea. Rev.*, **142,** 4519-4541, doi:10.1175/MWR-D-14-00100.1

Schneider, R. S., and A. R. Dean, 2008: A comprehensive 5-year severe storm environment climatology for the continental United States. Preprints, *24th Conf. on Severe Local Storms*, Savannah, GA, Amer. Meteor. Soc., 16A.4. [Available online at https://ams.confex.com/ams/24SLS/techprogram/paper_141748.htm.]

Schneider, R. S., A. R. Dean, S. J. Weiss, and P. D. Bothwell, 2006: Analysis of estimated environments for 2004 and 2005 severe convective storm reports. Preprints, *23rd Conf. on Severe Local Storms*, St. Louis, MO, Amer. Meteor. Soc., 3.5. [Available online at https://ams.confex.com/ams/pdfpapers/115246.pdf.]

Schumacher, R. S., and A. J. Clark, 2014: Evaluation of ensemble configurations for the analysis and prediction of heavy-rain-producing mesoscale convective systems. *Mon. Wea. Rev.*, **142**, 4108–4138, doi:10.1175/MWR-D-13-00357.1.

Schwartz, C. S., G. S. Romine, K. R. Smith, and M. L Weisman, 2014: Characterizing and optimizing precipitation forecasts from a convection-permitting ensemble initialized by a mesoscale ensemble Kalman filter. *Wea. Forecasting*, **29**, 1295–1318, doi:10.1175/WAF-D-13-00145.1.

Schwartz, C. S., G. S. Romine, M. L. Weisman, R. A. Sobash, K. R. Fossell, K. W. Manning, and S. B. Trier, 2015: A real-time convection-allowing ensemble prediction system initialized by mesoscale ensemble Kalman filter analyses. *Wea. Forecasting*, doi:10.1175/WAF-D-15-0013.1.

Schwartz, C. S., G. S. Romine, R. A. Sobash, K. R. Fossell, and M. L. Weisman, 2015: NCAR's Experimental Real-Time Convection-Allowing Ensemble Prediction System, *Wea. Forecasting*, **30,** 1645-1654, doi: https://doi.org/10.1175/WAF-D-15-0103.1.

Schwartz, C. S., M. Wong, Romine, G. S., Sobash, R. A., and Fossell, K. R., 2020: Initial Conditions for Convection-Allowing Ensembles over the Conterminous United States, *Mon. Wea. Rev.*, **148,** 2645-2669, doi: https://doi.org/10.1175/MWR-D-19-0401.1

Sherburn, K. D., and M. D. Parker, 2014: Climatology and ingredients of significant severe convection in high-shear, low-CAPE environments. *Wea. Forecasting*, **29**, 854–877, doi:10.1175/WAF-D-13-00041.1.

Sherburn, K. D., M. D. Parker, J. R. King, and G. M. Lackmann, 2016: Composite Environments of Severe and Nonsevere High-Shear, Low-CAPE Convective Events, *Wea. Forecasting*, **31,** 1899-1927. Retrieved Dec 1, 2021, from https://journals.ametsoc.org/view/journals/wefo/31/6/waf-d-16-0086_1.xml.

Skamarock, W. C., and Coauthors, 2019: A description of the Advanced Research WRF Model version 4. *NCAR Tech*. Note NCAR/TN-5565+STR, 162 pp., https://doi.org/10.5065/1dfh-6p97.

Smith, T. L., S. G. Benjamin, J. M. Brown, S. Weygandt, T. Smirnova, and B. Schwartz, 2008: Convection forecasts from the hourly updated, 3-km High Resolution

Rapid Refresh (HRRR) model. *24th Conf. on Severe Local Storms*, Savannah, GA, Amer. Meteor. Soc., 11.1. [Available online at https://ams.confex.com/ams/24SLS/techprogram/paper_142055.htm.]

Sobash, R. A., and J. S. Kain, 2017: Seasonal variations in severe weather forecast skill in an experimental convection-allowing model. *Wea. Forecasting*, **32**, 1885–1902, https://doi.org/10.1175/WAF-D-17-0043.1.

Thompson, R. L., R. Edwards, J. A. Hart, K. L. Elmore, and P. M. Markowski, 2003: Close proximity soundings within supercell environments obtained from the Rapid Update Cycle. *Wea. Forecasting*, **18**, 1243–1261, doi:10.1175/1520-0434(2003)018<1243:CPSWSE>2.0.CO;2.

Thompson, R. L., R. Edwards, and C. M. Mead, 2004: An update to the supercell composite and significant tornado parameters. Preprints, *22nd Conf. on Severe Local Storms*, Hyannis, MA, Amer. Meteor. Soc., P8.1. [Available online at https://ams.confex.com/ams/pdfpapers/82100.pdf.]

Thompson, G., P. R. Field, R. M. Rasmussen, and W. D. Hall, 2008: Explicit forecasts of winter precipitation using an improved bulk microphysics scheme. Part II: Implementation of a new snow parameterization. *Mon. Wea. Rev.*, **136**, 5095–5115, doi:10.1175/2008MWR2387.1.

Thompson, R., B. Smith, J. Grams, A. Dean, and C. Broyles, 2012: Convective modes for significant severe thunderstorms in the contiguous United States. Part II: Supercells and QLCS tornado environments. *Wea. Forecasting*, **27**, 1136–1154, https://doi.org/10.1175/WAF-D-11-00116.1.

Trier, S. B., F. Chen, and K. W. Manning, 2004: A study of convection initiation in a mesoscale model using high-resolution land surface initial conditions. *Mon. Wea. Rev.*, **132**, 2954–2976.

Trier, S. B., M. A. LeMone, F. Chen, and K. W. Manning, 2011: Effects of surface heat and moisture exchange on ARW-WRF warm-season precipitation forecasts over the central United States. *Wea. Forecasting*, **26**, 3–25.

Wasula, T. A., N. A. Stuart, and A. C. Wasula, 2008: The 17 February 2006 severe weather and high wind event across eastern New York and New England. Preprints, *24th Conf. on Severe Local Storms*, Savannah, GA, Amer. Meteor. Soc., 13B.3. [Available online at https://ams.confex.com/ams/24SLS/techprogram/paper_141699.htm.]